THE JOURNAL OF PHYSICAL CHEMISTRY C

Article

pubs.acs.org/JPCC

Molecular Engineering of Indoline-Based D−A−π−A Organic Sensitizers toward High Efficiency Performance from First-Principles Calculations

Wei-Lu Ding,[†] Dong-Mei Wang,[†,‡] Zhi-Yuan Geng,*[,†] Xiao-Ling Zhao,[†] and Yun-Feng Yan[†]

[†]Gansu Key Laboratory of Polymer Materials, College of Chemistry and Chemical Engineering, Key Laboratory of Eco-environment-related Polymer Materials, Ministry of Education, Northwest Normal University, Lanzhou, 730070 Gansu, People's Republic of China

[‡]Department of Chemistry, Baoji College of Arts & Sciences, Baoji, 721013 Shaanxi, People's Republic of China

Supporting Information

ABSTRACT: A series of new D−A−π−A indoline-based metal-free dyes, which are derived from the reported dye **WS-9**, have been designed and characterized theoretically for application in future dye-sensitized solar cells (DSSCs). The absorption, light harvesting efficiency, kinetics of charge injection, and recombination for all chromophores have been systematically investigated via first-principles calculations. We find that featuring the quinoxaline auxiliary acceptor instead of benzothiadiazole and modification on the −A acceptor (2-cyanoacrylic acid) with the −A1 acceptor (2,3-dicyanoacrylic acid) could result in a positive influence in dye **CDQ-A1** with respect to **WS-9**, which induces a remarkable enhancement of the parameters in close connection with the short-circuit current density (J_{sc}) as well as the open-circuit photovoltage (V_{oc}). In comparison to another **CDQ** dye, **CDQ-A4**, which differs from **CDQ-A1** by only the acceptor group, **CDQ-A1** displays outstanding performance due to its key parameters (i.e., absorption wavelength, light harvesting efficiency, dipole moment, less electron recombination) to achieve a balance between competing factors.

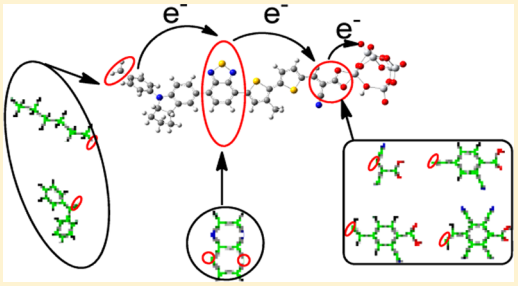

1. INTRODUCTION

Searching for clean and sustainable energy resources has aroused great interest in both scientists and engineers for the world. Huge efforts have been devoted in developing high efficient solar energy conversion technologies, and the most prospective approach is converting solar energy into electricity.[1−3] Since O'Regan and Grätzel first proposed dye-sensitized solar cells (DSSCs) in 1991,[4] DSSCs have attracted high interest over the last 20 years. As one of the most critical components in DSSCs, dye-sensitizers play a key function in the high conversion efficiency, which is responsible for light capturing and the generation of electric charges. Typically, the sensitizers are classified as metal complex and metal-free organic dyes. To date, the power conversion efficiency (η) of metal complexes (such as Ru dyes)-sensitized DSSCs holds the record at more than 11%.[5] However, ruthenium-complex dyes are not suitable for cost-effective and environmentally friendly photovoltaic systems due to that ruthenium is an expensive and rare metal, which may limit the potentially wide application of these complexes. As such, the exploration of DSSCs using pure organic dyes becomes very important from a practical point of view.

Thanks to researchers' remarkable efforts, high power conversion efficiency of pure organic dye-sensitized DSSCs has been achieved close to the ruthenium-complex dyes in experiments by some groups.[6−16] At the same time, major efforts via theoretical calculations have been taken to improve the cell performance by modifying the dye,[17−23] exploring the mechanisms of electron regeneration, injection, recombination,[24−31] as well as the intermolecular interaction in the dye/semiconductor (TiO_2)/electrolyte interfacial.[32−35] Commonly, most metal-free organic dyes have the "push−pull" structure of donor−π conjugated bridge−acceptor (D−π−A) where the photoinduced electron transfers from the donor part to the acceptor/anchoring group via the π-linkage. Here, motivated by the fact that the performances of metal-free dyes-sensitized DSSCs are various by minor modification, it is necessary to remodel the molecular design of organic sensitizers to provide insight into the physical origin underlying the relationship of structure and performance by using the state-of-the-art first-principles calculations. In this context, to further improve the performance of metal-free organic dyes theoretically, including not only the panchromatic light capturing, but also the critical parameters (i.e., light harvesting efficiency LHE, charge injection, and recombination, etc.) that govern the values of the short-circuit current (J_{sc}) and the open-current voltage (V_{oc}), we focus on increasing the capability of electron-donating on donor part, electron-transmission on auxiliary

Received: March 16, 2013
Revised: July 24, 2013
Published: July 31, 2013

   dx.doi.org/10.1021/jp402645h | J. Phys. Chem. C 2013, 117, 17382−17398

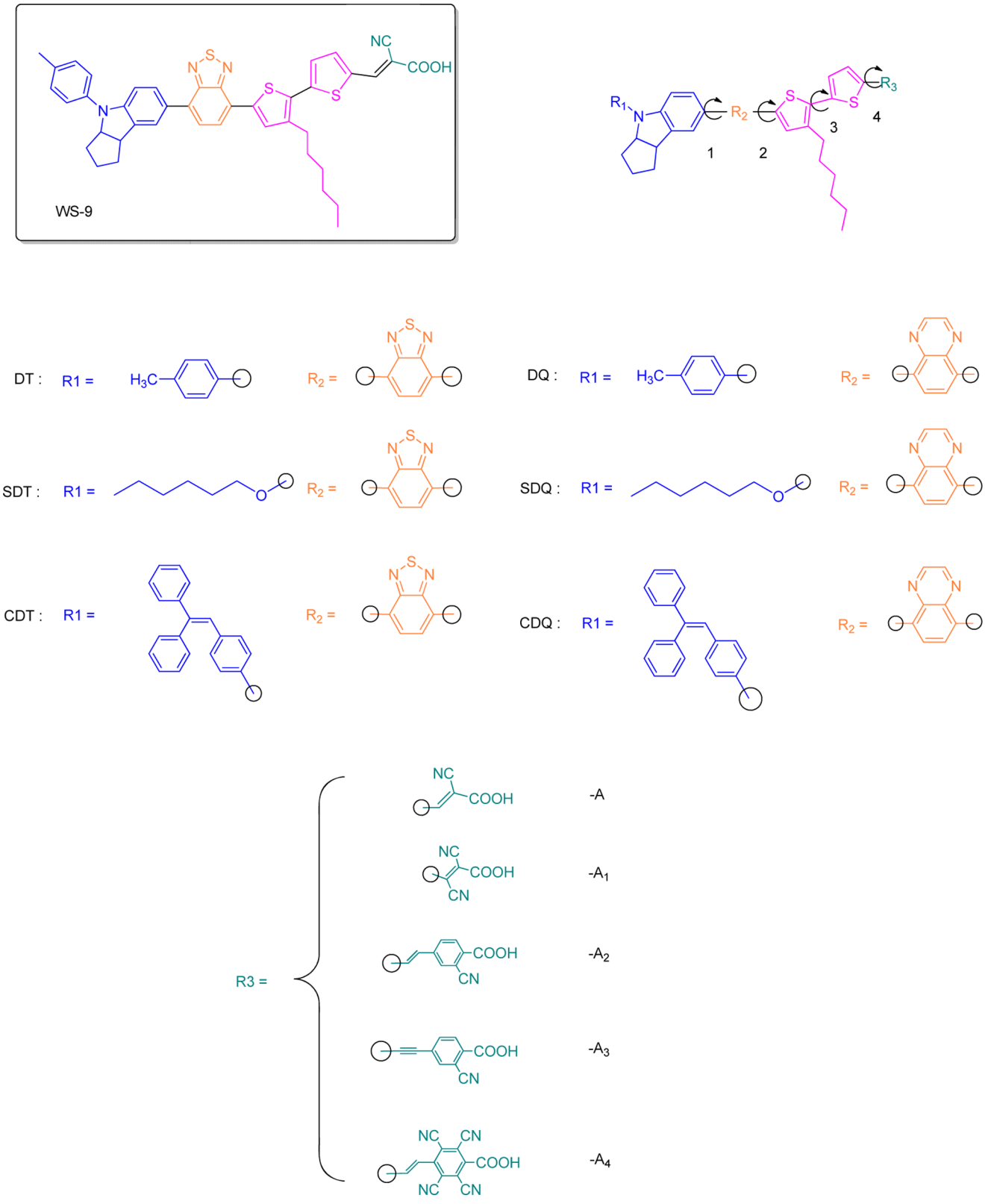

Figure 1. Target molecular structures based on different blocks in the D−A−π−A system (the black circles represent the binding sites).

acceptor, as well as electron-withdrawing on acceptor part, whereas we artificially fix the π bridge to construct the novel D−A−π−A architecture based on the reported dye **WS-9**.[9] This work suggests that with modifications to the auxiliary acceptor and acceptor group in our considered systems, the oxidation potential energy, maximum absorption peak, injection energy, orbital coupling, and dipole moment can be tuned significantly, but the modifying of the donor group could yields a subtle change as compared to **WS-9**. The fast screening toward a promising candidate based on the key parameters of light harvesting efficiency, charge injection, and recombination, as well as the intermolecular interaction of dye···I_2 adducts

dx.doi.org/10.1021/jp402645h | J. Phys. Chem. C 2013, 117, 17382−17398

could achieve a good balance for high efficiency. It is found that the dye **CDQ-A1** (Figure 1) is prominent with respect to **WS-9**, which induces a remarkable enhancement of the parameters in close connection with the short-circuit current density (J_{sc}) and the open-circuit photovoltage (V_{oc}). While for another **CDQ** dye, **CDQ-A4** differs from **CDQ-A1** by only the −A4 acceptor (four CN-substituted benzenoid ring), which possesses some comparable parameters as compared to **CDQ-A1**, the latter one is superior for application in future DSSCs due to it possessing less electron recombination from the conduction band to the redox couple (I^-/I^-_3) in the electrolyte. We hope our work could facilitate future experimental studies to design and fast screen new efficient organic dye-sensitizers.

2. METHOD

2.1. Theoretical Background. As we have known, the overall efficiency (η) of the DSSCs can be determined by the short-circuit current density (J_{sc}), the open-circuit photovoltage (V_{oc}), and the fill factor (ff), and it can be expressed by the following equation:[36]

$$\eta = \frac{J_{sc} V_{oc} ff}{P_{in}} \tag{1}$$

Correspondingly, the J_{sc} in DSSCs can be expressed as:[19]

$$J_{sc} = \int_{\lambda} \mathrm{LHE}(\lambda)\Phi_{inject}\eta_{collect}\, d\lambda \tag{2}$$

where LHE(λ) is the light harvesting efficiency at a given wavelength, Φ_{inject} denotes the electron injection efficiency, and $\eta_{collect}$ is the charge collection efficiency. First, based on eq 2, to obtain a high J_{sc}, the efficient organic dyes used in DSSCs should have a large LHE, which is described by:[37]

$$\mathrm{LHE} = 1 - 10^{-A} = 1 - 10^{-f} \tag{3}$$

where $A(f)$ is the absorption (oscillator strength) of the dye; the larger $A(f)$ could fulfill a better light capturing. For a DSSCs to work properly, it is clear that both ground-state oxidation potential energy (E^{dye}) and the excited-state oxidation potential energy (E^{dye*}) of the dyes have to match the redox potential (−4.8 eV vs vacuum) of the iodine/iodide electrolyte and the conduction band (−4.0 eV vs vacuum) of the TiO_2 electrode, respectively. They also could be evaluated via the following expression:[38]

$$E^{dye*} = E^{dye} - E_{00} \tag{4}$$

where E_{00} is the vertical transition energy. It is generally accepted that the electron injection from the photoinduced excited states of organic dyes to the semiconductor occurs before the vibrational relaxation.[39] Hence, in this case, E^{dye*} is estimated using the unrelaxed path. Furthermore, to inject the electron of the excited state efficiently, the lifetime τ of the excited state(s)[40,41] is an important factor for considering the efficiency of charge transfer. A dye with a longer lifetime in the excited state is expected to be more facile for charge transfer. In the present investigation, the τ value is approximately set to the lifetime of spontaneous luminescence, which is evaluated by:[40,41]

$$\tau = \frac{1}{A_{k,k'}} \tag{5}$$

$$A_{k,k'} = \frac{4e^2 \Delta E^3_{k',k}}{3\hbar^4 c^3} |r_{k,k'}|^2 \tag{6}$$

where $A_{k,k'}$ is the Einstein coefficient for spontaneous emission, e is the elementary charge, $\hbar$ is the reduced Planck's constant, and c is the speed of light in a vacuum. Moreover, $\Delta E_{k',k}$ and $r_{k,k'}$ represent the transition energy and transition dipole moment from states k to k', respectively. Besides the parameters mentioned above, the kinetics of the electron injection into the conduction band and the recombination from semiconductor to oxidized dyes should be taken into account because they largely influence the final conversion efficiency.[24,27] Thus, the analysis of the tendency of charge injection and recombination is critical to screen a new chromophore rapidly; see the corresponding elementary theory details in refs 24, 27, 42, 43. We only provide an outline of the classical theory in this work for the sake of fast screening. To evaluate charge injection and recombination based on the nonadiabatic electron transfer with modest computational expense, the dye adsorbed system is partitioned into three subsystems, the sensitizer molecule, the semiconductor surface, and the interface between the two. Accordingly, the three subunits of the model could be computed independently. Correspondingly, the dye−semiconductor coupling $\Gamma(E)$ can be written in terms of the coupling between atomic orbital on the sensitizer and delocalized orbitals on the semiconductor:[24,27,42]

$$\Gamma_{ss}(E) = \sum_{m,n} \Gamma_{mn}(E) c_m c_n^* \tag{7}$$

$$\Gamma_{mn}(E) = \frac{2\pi}{\hbar} \sum_{kk'} (ES_{mk} - V_{mk})(ES_{nk'} - V_{nk'})\rho_{kk'}(E) \tag{8}$$

$$\rho_{kk'}(E) = \sum_{l} C^*_{kl} C_{k'l} \delta(E - E_l) \tag{9}$$

where $\rho_{kk'}(E)$ is only dependent on the electrode and can be computed once for all molecules on a given surface, while V_{mk} is dependent on the dye−electrode interaction. Finally, evaluating the charge injection or recombination follows as : (i) a computation on the isolated sensitizer gives the molecular orbital coefficients c_m of LUMO or HOMO, (ii) a computation on the interface gives the coupling V_{mk} used to compute the self-energy $\Gamma_{mn}(E)$, and (iii) a computation on the electrode is used to obtain the local density of states $\rho_{kk'}(E)$ based on eq 7, respectively. Moreover, evaluation of the recombination rate constant can be expressed as:[42]

$$k_{CR} = \int_{CB} \Gamma(E) f(E - E_F) F(E, \Delta G, \lambda)\, dE \tag{10}$$

The terms appearing in the integral are the dye−semiconductor coupling $\Gamma(E)$, the Fermi−Dirac distribution f that depends on the quasi-Fermi level of the system ($E_{f,n}$), and the Franck−Condon term $F(E)$, which is the thermally averaged Franck−Condon integral between the initial and final vibrational wave functions. In addition, the explicit expression of the Franck−Condon $F(E)$ term in the high temperature limit is:[42]

$$F(E, \Delta G, \lambda) = \frac{1}{\sqrt{4\pi\lambda k_b T}} \exp\left[-\frac{(E + \Delta G + \lambda)^2}{4\lambda k_b T}\right] \tag{11}$$

dx.doi.org/10.1021/jp402645h | J. Phys. Chem. C 2013, 117, 17382−17398

Table 1. Effects of Functional on the Estimated Vertical Excitation Energy (Units in eV) of Dye WS-9 in CH_2Cl_2 Solution

	functional				
	BHandHLYP	CAM-B3LYP			
	6-31+G**	6-31+G**	6-31+G*	6-31G*	exp.[a]
cal.	561.7(2.21)	549.3(2.26)	561.7(2.21)	534.8(2.32)	536(2.31)

[a]Experimental value measured in CH_2Cl_2 solution from ref 9.

As a result, together with the function $\Gamma(E)$ and the thermal energy k_bT, key parameters that determine the recombination rate are the reorganization energy λ, and the energy difference ΔG between the initial (cation) and final (neutral) states for the molecular adsorbate, as well as the position of the conduction band minimum E, which controls the alignment of the adsorbate and semiconductor energy levels. For reorganization energy λ, it can be expressed as the following formula:[44]

$$\lambda_i = [E_0^{\pm} - E_{\pm}^{\pm}] + [E_{\pm}^{0} - E_0] \quad (12)$$

where $E_0^{\pm}$ is the energy of the cation or anion calculated with the optimized structure of the neutral molecule, $E_{\pm}^{\pm}$ is the energy of the cation or anion calculated with the optimized cation or anion structure, $E_{\pm}^{0}$ is the energy of the neutral molecule calculated at the cationic or anionic state, and E_0 is the energy of the neutral molecule at ground state, respectively.

As for V_{oc} in DSSCs, it could be described by:[45]

$$V_{oc} = \frac{E_{CB} + \Delta CB}{q} + \frac{k_bT}{q}\ln\left(\frac{n_c}{N_{CB}}\right) - \frac{E_{redox}}{q} \quad (13)$$

where E_{CB} is the conduction band edge of the semiconductor, E_{redox} is the electrolyte Fermi level, k_bT is the thermal energy, q is the unit charge, n_c is the number of electron in the conduction band, and N_{CB} is the accessible density of conduction band (CB) states. ΔCB is the shift of E_{CB} when the dyes are adsorbed on the semiconductor surface and can be expressed as:[19]

$$\Delta CB = -\frac{q\mu_{normal}\gamma}{\varepsilon_0\varepsilon} \quad (14)$$

where q is the electron charge, μ_{normal} is the component of dipole moment of the individual sensitizer perpendicular to the surface of semiconductor surface, γ is the dye's surface concentration, and ε_0 and ε are the permittivity of the vacuum and the dielectric constant of the organic monolayer. It is obvious from eqs 13 and 14 that a dye with large n_c and μ_{normal} would exert crucial influence on V_{oc}. In the eq 13, the sum of the first two terms is the quasi Fermi level in TiO_2; thus, the V_{oc} is the difference between the quasi Fermi level in TiO_2 and the E_{redox}.

In addition to the direct parameters that correlate closely to the conversion efficiency, understanding the nature and magnitude of the intermolecular interaction could be also helpful to elucidate why DSSCs sensitized by similar chromophores yield different efficiency. Therefore, the stabilization energy $E^{(2)}$ (kcal/mol) associated with $i \rightarrow j$ delocalization is taken into account to illustrate intermolecular interaction inherently and is explicity estimated by the following equation:[46]

$$E^{(2)} = \Delta E_{ij} = q_i\frac{F^2(i,j)}{\varepsilon_j - \varepsilon_i} \quad (15)$$

where q_i is the ith donor orbital occupancy, ε_i and ε_j are the diagonal elements (orbital energies), and $F(i,j)$ is the off-diagonal element associated with the NBO Fock matrix.

2.2. Atomistic Models and Computational Details. All calculations are conducted with density functional theory DFT and time-dependent density functional theory TD-DFT using the Gaussian 09 package.[47] The geometries of all isolated dyes in their neutral, cationic, and anionic states in the gas phase are fully optimized at hybrid DFT levels by B3LYP function[48] with the 6-31G* basis set.[49] Frequency calculations are performed on the fully optimized geometries; all predicted vibrational spectra have no imaginary frequency implying that optimized geometry is located at the lowest point of the potential energy surface. Optical absorption spectra at the ground-state optimized geometries for the 10 lowest singlet−singlet excitations are calculated using the TD-DFT method in conjunction with a conductor-like polarizable continuum model (C-PCM).[50] With the aim of checking the reliability, we use different XC functional (see Table 1), including BHandHLYP,[49] CAM-B3LYP,[51] combined with different basis sets to evaluate the effect of different functionals on the transition energies. Comparison between computational and experimental absorption spectra shows that the results given by the combination of TD-CAM-B3LYP with 6-31G* are in good agreement with the experimental values. The oxidation potentials of all of the isolated molecules of the ground state and excited state are carried out with the C-PCM-B3LYP/6-311G** level at the geometries of B3LYP/6-31G* level through single points calculations in their neutral and cationic calculated with the optimized structure of the neutral molecule. Furthermore, the stable structure of singlet excited state (S_1) is optimized at the extra DFT calculations after the screened chromophores adsorbed on the $(TiO_2)_6$ cluster to evaluate the atomic charge distribution and the charge transfer from S_0 to S_1 state and lucubrated by using electron density differences maps (EDDMs) implemented in Multiwfn 3.0.1.[52,53] Absorption spectra of adsorbed systems are simulated by C-PCM-CAM-B3LYP/6-31G* (LANL2DZ basis set[54] for Ti atom) to examine the influence of the interfacial interaction between the dye and $(TiO_2)_6$ cluster on the electron excitation. In addition, the calculations of the intermolecular interaction between the dye···I_2 complexes are performed by the B3LYP function (LANL2DZ basis set for I atom and 6-31G* basis set for other atoms), and the natural bond orbital (NBO) analysis[46] is carried out at the optimized dye···I_2 structures to elucidate the electron recombination losses. All dyes we calculated are a simplified model of Figure 1, in which the long hexyl chain at π-linker and the hexyloxy group at the donor are replaced by methyl group and methoxy group, respectivly, which have been proved to not influence the electronic properties of the dyes in our previous work,[55] and the details in are in section 3.1.

dx.doi.org/10.1021/jp402645h | J. Phys. Chem. C 2013, 117, 17382−17398

3. RESULTS AND DISCUSSION

3.1. Molecular Design. The current maximum efficiency of pure organic dye-sensitized DSSC recorded for DSSCs is 11%, while the theoretical maximum achievable according to macroscopic models should be around 30%.[56] To improve the efficiency of the cell, we aim to design more efficienct dye-sensitizers via theoretical calculation before the synthesis and the device fabrication. The other components (i.e., different semiconductors and their morphologies, redox pairs in electrolyte, solid-state substitutes of the electrolyte solution) optimized would provide further interesting insight on the DSSCs, but they are beyond the scope of this work. Generally, the modifications on sensitizers focus on improving the capability of electron-transmission of π-linker and electron-withdrawing of the acceptor. The common dyes with D−π−A configuration-based DSSCs have been examined and shown not to achieve high conversion efficiency, while, based on a variety of experiments[9,10,14,57−61] and our calculation before,[55] the D−A−π−A construction is superior to the D−π−A configuration, and, therefore, is considered in this work to build new sensitizers. We artificially fix the conjunction linkage, bithiophene (due to that long π-conjugated dye molecules easily form unfavorable π-stacks and are not very stable when irradiated with high-energy photos), and systematically analyze the influence of the variation of donor group, auxiliary acceptor, and acceptor segments (see Figure 1). To save computational expense, we use the simplified model, in which the long hexyl chain at π-linker and the hexyloxy group at the donor part are replaced by methyl and methoxy, respectively. The total density-of-states (DOS) and partial density-of-states (PDOS) spectra in Supporting Information Figure S1 point out that the contribution from hexyl and hexyloxy (blue) to whole molecule (pink) could be negligible from the range of H-10→L+10, indicating that the simplified model is reliable in our work. A final minor complication, to elucidate the main purpose of using the long hexyloxy and hexyl attached on molecular backbone, is to gain better rectification in experiment, the simplified and unsimplified models of the dimers in **WS-9** and **SDT-A** are simulated, and the results are plotted in Supporting Information Figure S2. Obviously, the dimers of the unsimplified models suggest that attaching hexyloxy and hexyl on the backbone could enlarge the intermolecular distances, and therefore weaken the tendency of π−π interaction and aggregation. The NBO atomic charge distributions of carboxyl in Supporting Information Table S2 indicate that the electron loss of intermolecular interaction is demerit for charge transfer, thus elucidating that attaching hexyloxy and hexyl into the molecular backbone is critical, and our results show that using the simplified model is reliable in our calculations.

3.2. Absorption of the Designed Chromophores. Theoretically, the prerequisite for dye-sensitizers used in DSSC to work properly is that the HOMO levels have to be lower than that of the iodine/iodide electrolyte (−4.8 eV vs vacuum) and LUMO levels have to be higher than that of the conduction band of the TiO_2 electrode (−4.0 eV vs vacuum), respectively. Commonly, based on Koopman's theorem, the ground-state oxidation potential energy (E^{dye}) and the excited-state oxidation potential energy (E^{dye}*) could be estimated as negative HOMO and negative LUMO energy levels approximately, and the approximation is in fair agreement with experimental tendency, but is not precise enough. To be more quantitative, the oxidation potential energy (Table 2) and the energy levels (Supporting Information Figure S3) are combined to elucidate the difference of absorption. It is clear that all of these newly designed dyes are satisfied with the requirement of a sensitizer utilized in DSSC potentially. So, we begin the discussion of absorption in sections 3.2.1−3.2.6.

Table 2. Evaluated Oxidation Potential of All Dyes (Units in eV)

dyes	E^{dye}	E^{dye}*	dyes	E^{dye}	E^{dye}*
WS-9	5.07 (0.66 V)[a]	2.75 (−1.39 V)[a]	**DQ-A**	5.06	2.55
DT-A1	5.11	2.97	**DQ-A1**	5.10	2.85
DT-A2	4.99	2.63	**DQ-A2**	4.99	2.42
DT-A3	5.01	2.62	**DQ-A3**	5.01	2.38
DT-A4	5.06	2.93	**DQ-A4**	5.06	2.84
SDT-A	5.00	2.70	**SDQ-A**	4.99	2.50
SDT-A1	5.04	2.92	**SDQ-A1**	5.03	2.80
SDT-A2	4.93	2.59	**SDQ-A2**	4.93	2.38
SDT-A3	4.95	2.58	**SDQ-A3**	4.95	2.34
SDT-A4	5.00	2.89	**SDQ-A4**	4.99	2.79
CDT-A	5.04	2.71	**CDQ-A**	5.03	2.52
CDT-A1	5.08	2.93	**CDQ-A1**	5.06	2.80
CDT-A2	4.97	2.61	**CDQ-A2**	4.98	2.41
CDT-A3	4.99	2.59	**CDQ-A3**	4.99	2.36
CDT-A4	5.04	2.89	**CDQ-A4**	5.03	2.81

[a]Data are experimental values from ref 9.

3.2.1. DT Series of Dyes. Organic dyes with the electron-rich block (triphenylamine, indoline, coumarine, carbazole, etc.) as the donor part and the electron-deficient carboxylate-cyanoacrylic as the acceptor/anchoring group have been applied in real devices successfully. In general, the absorption could be tuned by means of introducing some functional groups into the molecular skeleton from the electronic structure point of view. Commonly, the E^{dye} in dye-sensitizer could govern the regeneration for the oxidized dye by the I^-/I^-_3 redox couple after electron injection into the TiO_2 conduction band, and the energy gap of HOMO→LUMO orbitals determines the maximum absorption region in UV−vis. Therefore, we begin our investigation with the possibility of featuring different electron-deficient moieties from −A1 to −A4 (Figure 1) instead of 2-cyanoacrylic acid (−A) in **WS-9**, respectively, which function as the acceptor/anchoring group (denoted **DT** dyes), and examine the dependence of dye absorption transitions on these groups. For this family, the substitute of different acceptors in **WS-9** makes the variations of E^{dye} smaller than those of E^{dye}*, and a similar result is also observed between the HOMO and LUMO levels in Supporting Information Figure S3a. The simulated UV−vis for **DT** dyes is plotted in Figure 2a, and the corresponding absorption data are listed in Table 3. It is clear that this family shows three absorption bands: (i) the lower energy absorption band, which is ascribed to the intermolecular charge transfer (ICT) for all dyes, mainly corresponds to the H→L transition (S1 transition), although the transitions from other orbitals also make contributions; (ii) the additional absorption band around 400 nm (S2 transition) is raised in **WS-9**, **DT-A2**, and **DT-A3**, while it disappeared in **DT-A1** and **DT-A4**; and (iii) the higher

dx.doi.org/10.1021/jp402645h | J. Phys. Chem. C 2013, 117, 17382−17398

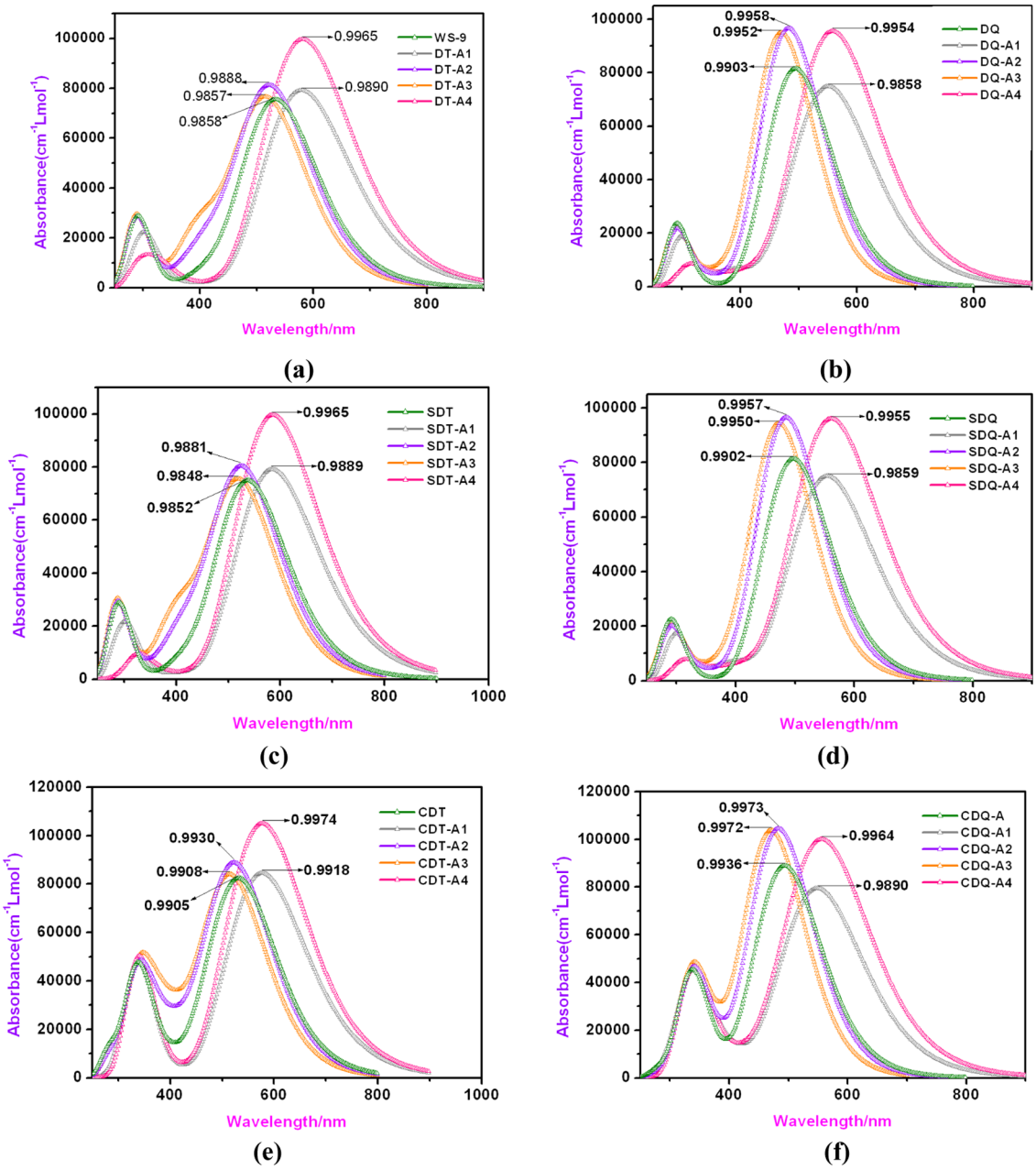

Figure 2. UV−vis absorption spectra and corresponding light-harvesting efficiency (LHE) values with (a) **DT**, (b) **DQ**, (c) **SDT**, (d) **SDQ**, (e) **CDT**, and (f) **CDQ** dyes calculated in CH_2Cl_2 solution.

excited states hopping such as H→L+2, H→L+4, and H→L+5 contribute to the absorption band in the UV region. It is interesting to note that the absorption region of **DT-A1** and **DT-A4** is broadened and their ICT band is red-shifted to around 580 nm (both red shift ∼50 nm with respect to **WS-9**) in CH_2Cl_2 solution, and the absorption onset is extended ∼70 nm to the near-infrared (NIR) region from 830 nm (**WS-9**) to 900 nm (**DT-A1** and **DT-A4**), which increases the incident photon to current conversion efficiency (IPCE) potentially. On the contrary, the ICT bands of **DT-A2** and **DT-A3** both are blue-shifted ∼10 nm as compared to **WS-9**, and the absorption onsets present an identical blue-shift that could be explained by the larger dihedral angles 3 (see Figure 1 and Supporting Information Table S1) formed by the bithiophene unit and the acceptor/anchoring derivatives, as a result, weaken the charge migration. Meanwhile, the subtle difference of absorption in **DT-A2** and **DT-A3** suggests that almost the same efficiency could be obtained in −CH═CH− and −CH≡CH− groups. The above analysis confirms again that the modifications on the acceptor would display a significant effect on the electron excitation. Aside from the absorption, we prefer to get insight into the corresponding LHE value of dye-sensitizer, which is closest to the magnitude of the oscillator strength *f*. Apparently, featuring the different acceptors instead of the 2-cyanoacrylic acid in **WS-9** exhibits various oscillator strength *f*. As follows from Figure 2a, **DT-A1** and **DT-A4** exhibit larger oscillator strength with respect to **WS-9**, and achieve an improved LHE (the relative LHE[62] (Supporting Information Table S3) of 0.9128 and 0.9530, respectively). In addition, a further calculation using eqs 5 and 6 shows that lifetime τ of the first excited state of **DT-A1** should be longer than other sensitizers thanks to its relative smaller excitation energy $\Delta E_{k',k}$ and

dx.doi.org/10.1021/jp402645h | J. Phys. Chem. C 2013, 117, 17382−17398

Table 3. Electronic Transition Data Obtained by C-PCM-CAM-B3LYP/6-31G* Level for Each Molecule in the CH_2Cl_2 Solution with the B3LYP/6-31G* Geometries[a]

dyes	energy (eV)	transition character[b]	f	λ_{max}/nm	$r_{k,k'}$[c]
WS-9	2.32($S_0 \rightarrow S_1$)	H→L(68.8%)	1.8477	534.8	32.5313
	2.93($S_0 \rightarrow S_2$)	H→L+1(43.6%)	0.1936	423.4	
	4.15($S_0 \rightarrow S_5$)	H→L+2(38.0%)	0.3792	298.5	
DT-A1	2.14($S_0 \rightarrow S_1$)	H→L(54.4%)	1.9572	579.3	37.3225
	4.01($S_0 \rightarrow S_6$)	H→L+2(39.0%)	0.2975	309.2	
DT-A2	2.36($S_0 \rightarrow S_1$)	H→L(77.9%)	1.9525	526.3	33.8305
	2.94($S_0 \rightarrow S_2$)	H→L+1(38.6%)	0.4532	421.5	
	4.27($S_0 \rightarrow S_7$)	H→L+4(26.8%)	0.4417	290.2	
DT-A3	2.39($S_0 \rightarrow S_1$)	H→L(75.7%)	1.8453	518.8	31.5186
	3.03($S_0 \rightarrow S_2$)	H−1→L(42.9%)	0.5780	409.4	
	4.29($S_0 \rightarrow S_7$)	H→L+4(22.5%)	0.3564	288.7	
DT-A4	2.13($S_0 \rightarrow S_1$)	H→L(39.4%)	2.4541	581.8	47.0070
	3.80($S_0 \rightarrow S_7$)	H→L+3(40.8%)	0.1954	326.4	
	4.27($S_0 \rightarrow S_{10}$)	H→L+5(27.1%)	0.2098	290.6	
DQ-A	2.51($S_0 \rightarrow S_1$)	H→L(51.8%)	2.0137	494.6	32.8071
	4.26($S_0 \rightarrow S_7$)	H→L+2(34.1%)	0.4635	291.1	
DQ-A1	2.25($S_0 \rightarrow S_1$)	H→L(45.0%)	1.8480	550.9	33.5385
	4.16($S_0 \rightarrow S_9$)	H→L+2(26.3%)	0.2274	297.9	
DQ-A2	2.57($S_0 \rightarrow S_1$)	H→L(57.2%)	2.3791	483.1	37.8358
	4.11($S_0 \rightarrow S_6$)	H→L+1(19.0%)	0.1943	301.5	
	4.32($S_0 \rightarrow S_8$)	H→L+5(25.6%)	0.3173	286.8	
DQ-A3	2.63($S_0 \rightarrow S_1$)	H→L(51.1%)	2.3231	471.2	36.0386
	4.14($S_0 \rightarrow S_6$)	H→L+1(22.7%)	0.2195	299.2	
	4.34($S_0 \rightarrow S_8$)	H→L+5(30.6%)	0.3333	285.4	
DQ-A4	2.22($S_0 \rightarrow S_1$)	H→L(31.7%)	2.3357	559.2	43.0023
	3.96($S_0 \rightarrow S_9$)	H→L+3(28.1%)	0.1557	313.2	
SDT-A	2.30($S_0 \rightarrow S_1$)	H→L(66.8%)	1.8301	539.5	32.5053
	2.91($S_0 \rightarrow S_2$)	H→L+1(41.5%)	0.2182	426.2	
	4.15($S_0 \rightarrow S_5$)	H→L+2(34.8%)	0.3179	298.8	
SDT-A1	2.12($S_0 \rightarrow S_1$)	H→L(53.2%)	1.9534	584.8	37.6101
	3.99($S_0 \rightarrow S_6$)	H→L+2(43.7%)	0.3164	310.7	
	4.37($S_0 \rightarrow S_{10}$)	H−7→L+1(33.8%)	0.1461	284.0	
SDT-A2	2.34($S_0 \rightarrow S_1$)	H→L(75.2%)	1.9253	529.4	33.5567
	2.93($S_0 \rightarrow S_2$)	H−1→L(39.1%)	0.4847	423.5	
	4.28($S_0 \rightarrow S_7$)	H→L+4(24.0%)	0.4123	290.0	
SDT-A3	2.37($S_0 \rightarrow S_1$)	H→L(73.2%)	1.8175	522.8	31.2809
	3.01($S_0 \rightarrow S_2$)	H−1→L(43.8%)	0.6082	411.6	
	4.29($S_0 \rightarrow S_7$)	H→L+5(30.2%)	0.3469	289.0	
SDT-A4	2.11($S_0 \rightarrow S_1$)	H→L(37.9%)	2.4538	586.3	47.3622
	3.78($S_0 \rightarrow S_7$)	H→L+3(39.4%)	0.1812	327.9	
SDQ-A	2.49($S_0 \rightarrow S_1$)	H→L(49.7%)	2.0089	497.5	32.9027
	4.26($S_0 \rightarrow S_7$)	H→L+2(34.4%)	0.4389	291.2	
SDQ-A1	2.23($S_0 \rightarrow S_1$)	H→L(44.2%)	1.8518	554.9	33.8254
	3.16($S_0 \rightarrow S_3$)	H→L+1(41.6%)	0.1564	392.0	
	4.12($S_0 \rightarrow S_8$)	H−9→L(27.8%)	0.1887	300.7	
SDQ-A2	2.55($S_0 \rightarrow S_1$)	H→L(52.8%)	2.3706	485.7	37.9033
	4.09($S_0 \rightarrow S_6$)	H−1→L+2(22.6%)	0.1798	303.5	
	4.33($S_0 \rightarrow S_8$)	H→L+5(20.9%)	0.2972	286.7	
SDQ-A3	2.61($S_0 \rightarrow S_1$)	H→L(47.8%)	2.3011	474.2	35.9202
	4.11($S_0 \rightarrow S_6$)	H→L+1(23.1%)	0.2007	301.5	
	4.35($S_0 \rightarrow S_8$)	H→L+5(23.9%)	0.3081	285.2	
SDQ-A4	2.20($S_0 \rightarrow S_1$)	H→L(29.9%)	2.3501	562.4	43.5072
	3.94($S_0 \rightarrow S_9$)	H→L+3(28.7%)	0.1496	314.5	
CDT-A	2.33($S_0 \rightarrow S_1$)	H→L(60.5%)	2.0234	532.5	35.4720
	2.93($S_0 \rightarrow S_2$)	H→L+1(37.0%)	0.1329	423.0	
	3.66($S_0 \rightarrow S_4$)	H→L+2(65.9%)	1.1108	338.3	
CDT-A1	2.15($S_0 \rightarrow S_1$)	H→L(47.3%)	2.0884	577.1	39.6762
	3.54($S_0 \rightarrow S_4$)	H−1→L+1(43.6%)	0.3495	350.5	
	3.69($S_0 \rightarrow S_5$)	H→L+3(35.9%)	0.8349	335.7	
CDT-A2	2.36($S_0 \rightarrow S_1$)	H→L(71.5%)	2.1521	525.7	37.2434

dx.doi.org/10.1021/jp402645h | J. Phys. Chem. C 2013, 117, 17382−17398

Table 3. continued

dyes	energy (eV)	transition character[b]	f	λ_{max}/nm	$r_{k,k'}$[c]
	2.94($S_0 \rightarrow S_2$)	H→L+1(34.2%)	0.3394	421.3	
	3.66($S_0 \rightarrow S_4$)	H→L+3(52.7%)	0.9596	339.0	
CDT-A3	2.40($S_0 \rightarrow S_1$)	H→L(68.8%)	2.0358	517.5	34.6812
	3.03($S_0 \rightarrow S_2$)	H−1→L(38.5%)	0.4545	409.3	
	3.67($S_0 \rightarrow S_4$)	H→L+3(58.2%)	0.9290	338.1	
CDT-A4	2.15($S_0 \rightarrow S_1$)	H→L(32.6%)	2.5850	577.8	49.1675
	3.66($S_0 \rightarrow S_7$)	H→L+4(53.2%)	0.9320	339.2	
CDQ-A	2.51($S_0 \rightarrow S_1$)	H→L(43.1%)	2.1963	493.8	35.7027
	3.67($S_0 \rightarrow S_4$)	H→L+2(64.6%)	1.0670	338.3	
CDQ-A1	2.26($S_0 \rightarrow S_1$)	H→L(37.2%)	1.9591	549.1	35.4146
	3.19($S_0 \rightarrow S_3$)	H→L+1(36.3%)	0.2235	388.9	
	3.63($S_0 \rightarrow S_4$)	H→L+2(53.0%)	0.8369	341.4	
CDQ-A2	2.57($S_0 \rightarrow S_1$)	H→L(49.3%)	2.5764	483.3	40.9905
	3.51($S_0 \rightarrow S_3$)	H−1→L+1(47.2%)	0.4115	353.6	
	3.69($S_0 \rightarrow S_4$)	H→L+3(45.3%)	0.7238	336.0	
CDQ-A3	2.63($S_0 \rightarrow S_1$)	H→L(43.9%)	2.5488	471.5	39.5589
	3.55($S_0 \rightarrow S_3$)	H−1→L+1(44.6%)	0.5221	349.6	
	3.70($S_0 \rightarrow S_4$)	H→L+3(43.9%)	0.6177	335.2	
CDQ-A4	2.22($S_0 \rightarrow S_1$)	H→L(25.2%)	2.4406	557.7	44.8074
	2.91($S_0 \rightarrow S_3$)	H→L+2(48.6%)	0.1273	426.5	
	3.57($S_0 \rightarrow S_6$)	H−1→L+2(34.9%)	0.5944	347.1	

[a]H represents HOMO, L represents LUMO. [b]Data in parentheses are the main configurations. [c]Units in debye.

transition dipole moment $r_{k,k'}$, which is meriting for higher τ of the first excited state in electron injection from the sensitizer to the semiconductor. Moreover, as mentioned above, the S2 transition in **DT-A1** and **DT-A4** that disappeared may be attributed to the negligible second transition dipole moment (see Supporting Information Table S4), implying that minor modification renders a large influence on transition dipole moment, and subsequently influence the absorption directly. Consequently, **DT-A1** and **DT-A4** could red shift the maximum absorption peak, improve the LHE, and **DT-A1** would render the longer lifetime τ of the first excited state.

3.2.2. DQ Series of Dyes. In the reported works, incorporating an additional electron-withdrawing segment in D−A−π−A architecture could favor the electron transfer, and some groups as the auxiliary acceptor (benzotriazole, benzothiazole, quinoxaline, etc.) have been detected and applied in real devices successfully. Thus, we design another series (coded as **DQ**) by substituting the benzothiadiazole in the **DT** family using the quinoxaline to examine the two auxiliary acceptors dependence on the photophysical properties. The variations of E^{dye*} and LUMO level in **DQ** family are a bit larger than those of E^{dye} and HOMO level, which implicates the effect of auxiliary acceptor on the E^{dye*} and LUMO level but E^{dye} and HOMO level. Figure 2b displays the similar ICT bands between **DQ** and **DT** dyes, of which the lower energy absorption band (S1 transition) for all **DQ** dyes mainly corresponds to the H→L transition. Interestingly, the additional absorption band around 400 nm (S2 transition) in all **DQ** dyes disappeared, which may be attributed to the negligible second transition dipole moment (Supporting Information Table S4). Moreover, the absorption band around 300 nm is composed of the higher excited states hopping, that is, S6, S7, S8, and S9. At the same time, the maximum absorption peak of **DQ-A1** and **DQ-A4** is red-shifted to ∼550 nm and blue-shifted to ∼480 nm in the **DQ-A2** and **DQ-A3** as compared to **DQ-A** (∼490 nm). Overall, the absorption of **DQ** family is blue-shifted with respect to **DT** family because less planarity in the whole molecular backbone of **DQ** dyes decreases the fast transfer of the photoinduced electron in the intramolecule. Remarkably, the oscillator strength f of **DQ-A1** and **DQ-A4** is smaller than their counterparts **DT-A1** and **DT-A4**, and subsequently decreases the LHE to some extent (RLHE of 0.8863 and 0.8883, respectively). Furthermore, the LHE of **DQ-A2** and **DQ-A3** is not only larger than the **DQ-A1** and **DQ-A4**, but also superior to the **DT-A2** and **DT-A3** counterparts; the rational explanations are the comparable oscillator strength f as compared to **DQ-A1** and **DQ-A4**, and also smaller dihedral angle 3 as compared to **DT-A2** and **DT-A3**, respectively. On the other hand, the change tendency of lifetime τ of the first excited state in **DQ** dyes points out that transition dipole moment $r_{k,k'}$ becomes larger in **DQ-A**, **DQ-A2**, and **DQ-A3** in comparison to **DT-A**, **DT-A2**, and **DT-A3**, respectively. Combined with the larger excitation energy $\Delta E_{k',k}$, **DQ-A**, **DQ-A2**, and **DQ-A3** diminish the lifetime τ of the first excited state and the efficiency of excited electron injection. As a whole, dye **DQ-A1** and **DQ-A4** perform well upon the replacement of the benzothiadiazole with quinoxaline in **DT-A1** and **DT-A4** as evidenced by the comparable LHE and longer lifetime τ of the first excited state.

3.2.3. SDT Series of Dyes. Besides the modifications on the acceptor and auxiliary acceptor segments, another way to bathochromically shift the absorption peak is to increase the electron-donating capability of the donor part. Employing this strategy, the possibility of building an alkyloxy chain in the donor part of **DT** family is taken into account to investigate their photophysical properties dependence on the additional electron-donating ability. Oxidation potential and ΔE_{H-L} reveal that the subtle red-shift obtained in the **SDT** set because of the HOMOs is heightened slightly, while the LUMOs maintain almost no change as compared to **DT** dyes. Figure 2c plots the absorption spectra; it reproduced well with the change tendency of ΔE_{H-L}, the red-shift of which is observed in **SDT-A1** and **SDT-A4**, while there is a blue-shift in **SDT-A2** and **SDT-A3**. Overall, all **SDT** dyes display a subtle

dx.doi.org/10.1021/jp402645h | J. Phys. Chem. C 2013, 117, 17382−17398

bathochromic (∼5−10 nm) as compared to **DT** dyes. Meanwhile, the oscillator strength f of **SDT** dyes is comparable to the **DT** set; consequently, LHEs are almost identical between the two families, which suggests that the introduction of alkyoxy in **SDT** dyes could not display a remarkable improvement in absorption and light capturing as compared to **DT** dyes. However, more excited states hopping (H−1→L, H−7→L+1) has been found in the **SDT** set, which indicates that more occupied molecular orbitals could be stimulated via adding an electron-donating group, albeit the prominent red-shift has not been observed. Furthermore, the excitation energy $\Delta E_{k',k}$ and transition dipole moment $r_{k,k'}$ predict that the first excited lifetime τ of **SDT** family would be comparable to **DT** dyes due to the almost identical $\Delta E_{k',k}$ and $r_{k,k'}$ between the two sets.

3.2.4. SDQ Series of Dyes. To optimize the parameter of LHE that correlates to the short-circuit current density (J_{sc}) of the **SDT** family, the benzothiadiazole is replaced by quinoxaline unit to construct the **SDQ** family. Figure 2d shows that the maximum peak of all **SDQ** dyes is blue-shifted as compared to the **SDT** set, and the reason is similar to **DQ** dyes. The S2 transition could not be observed in Table 3, which is ascribed to the same reason of degraded second transition dipole moment. Moreover, the oscillator strength f of **SDQ-A1** and **SDQ-A4** is larger than **SDQ-A**, **SDQ-A2**, and **SDQ-A3**, while it is smaller than that of **SDT-A1** and **SDT-A4**. As a consequence, the LHE of **SDQ** dyes shows the same change tendency with the variation of oscillator strength f. However, the contribution from the lower ocuppied orbital to the transition is found (i.e., H−9→L), implying that the replacement of additional acceptor in **SDQ** family could trigger more excited state hopping, and as such overlap more with the solar radiation. Additionally, the result of the tendency of the first excited-state lifetime τ in **SDQ** molecules follows the same pattern as **DQ** sets, in which the $r_{k,k'}$ gets larger in **SDQ-A**, **SDQ-A2**, and **SDQ-A3**, while it shows the opposite result in **SDQ-A1** and **SDQ-A4** as compared to **SDT** dyes. As such, **SDQ-A1** and **SDQ-A4** present more efficient absorption, potential high IPCE, and longer first excited-state lifetime τ.

3.2.5. CDT Series of Dyes. To determine the efficient electron-donating group further, an ethane-1,1-diyldibenzene moiety (incorporated previously in dye **D149**[63]) is capped into **DT** series, and we repeat the characterization of absorption following the same pattern as before. On the basis of Figure 2e, the maximum absorption peak of **CDT** dyes is comparable to that of **DT** and **SDT** families, and from Table 3, the higher excited states hopping is similar to that of **SDT** chromophores. The oscillator strength f of the lower and higher energy absorption bands of **CDT** molecules becomes stronger than those of the **DT** and **SDT** families, which accordingly improves the LHEs with respect to **DT** (RLHEs range from 0.9116 to 0.9212) and **SDT** (RLHEs range from 0.9116 to 0.9242) families, respectively. Meanwhile, the first excited-state lifetime τ should be shortened in the **CDT** set due to the $\Delta E_{k',k}$ and $r_{k,k'}$ all presenting larger values than those of **DT** and **SDT** molecules, subsequently decreasing the IPCE potentially. Overall, dyes **CDT-A1** and **CDT-A4** are superior to other sensitizers in this set.

3.2.6. CDQ Series of Dyes. Last, **CDQ** series by featuring the quinoxaline instead of the benzothiadiazole in **CDT** series are built, to screen out the best candidate from the absorption point of view. As follows from Figure 2f and Table 3, it is noted that the maximum peak of **CDQ** series shows a subtle blue-shift as compared to the **DQ** and **SDQ** series, and a similar transition contribution is observed in comparison to **DQ** and **SDQ** series as well. Yet, the oscillator strength f of the corresponding lower and higher energy absorption bands of **CDQ** chromophores is stronger than that of **DQ** and **SDQ** dyes, which consequently improves the LHEs with respect to **DQ** (RLHEs range from 0.9129 to 0.9200) and **SDQ** (RLHEs range from 0.9085 to 0.9220) families, respectively. Furthermore, the result of the first excited-state lifetime τ of **CDQ** sensitizers follows the same pattern with the **CDT** series that is shortened as compared to **DQ** and **SDQ** sets due to the larger $\Delta E_{k',k}$ and $r_{k,k'}$ obtained. As a whole, dyes **CDQ-A1** and **CDQ-A4** are outstanding in this series.

3.3. Evaluating the Tendency of Charge Injection. As we know, a dye that performed well on the fast charge injection should couple strongly between the anchoring group of the dye and the semiconductor, and it has been verified by Troisi et al. that this coupling is determined by the LUMO orbital weight of the dye on the atoms of the carboxylic group.[24] Meanwhile, changing injection energy E_s and localization of the LUMO of some chromophores with the structural rigidity could induce the variation of the rate of injection.[24] Furthermore, the replacement of energy level with respect to the TiO_2 could affect the injection rate largely as well. As mentioned in Theoretical Background, the adsorbed system is partitioned into the isolated sensitizer, the semiconductor surface, and the interface between the two; thus, the items of molecular orbital coefficients c_m of LUMO, local density of states $\rho_{kk'}(E)$ of TiO_2, and molecule−electrode coupling V_{mk}, which correlate to the three subunits, are characterized to predict the tendency of charge injection. It has been pointed out that the sensitizers sharing the same adsorption chemistry showed similar coupling.[18,24] Subsequently, we assume that the V_{mk} and $\rho_{kk'}(E)$ of our considered systems are comparable due to that the sensitizers all possess the same anchoring group and graft on the same semiconductor surface. Consequently, the calculation of injection energy E_s and LUMO orbital weight of the dye on the atoms of the carboxylic group only relates to isolated dyes; the results are listed in Table 4. One can note that the −A1 or −A4 moiety featured chromophores in every family possess the smaller injection energy E_s than that of other dyes, and generally a very low injection energy would influence

Table 4. Computed Injection Energy E_s (Energy for the Dye's LUMO) and Quality Factor Q_{LUMO} for All Dyes

dyes	E_s/eV	Q_{LUMO} (%)	dyes	E_s/eV	Q_{LUMO} (%)
WS-9	−2.82	3.00	**DQ-A**	−2.68	5.06
DT-A1	−3.19	6.90	**DQ-A1**	−3.14	7.84
DT-A2	−2.67	2.44	**DQ-A2**	−2.53	5.77
DT-A3	−2.67	2.48	**DQ-A3**	−2.52	6.71
DT-A4	−3.30	4.73	**DQ-A4**	−3.27	4.80
SDT-A	−2.79	3.09	**SDQ-A**	−2.66	5.16
SDT-A1	−3.17	6.95	**SDQ-A1**	−3.12	7.86
SDT-A2	−2.64	2.63	**SDQ-A2**	−2.51	5.99
SDT-A3	−2.64	2.70	**SDQ-A3**	−2.50	7.04
SDT-A4	−3.28	4.77	**SDQ-A4**	−3.26	4.81
CDT-A	−2.85	2.90	**CDQ-A**	−2.71	4.92
CDT-A1	−3.21	6.84	**CDQ-A1**	−3.16	7.80
CDT-A2	−2.71	2.21	**CDQ-A2**	−2.56	5.41
CDT-A3	−2.70	2.25	**CDQ-A3**	−2.54	6.22
CDT-A4	−3.31	4.67	**CDQ-A4**	−3.29	4.77

dx.doi.org/10.1021/jp402645h | J. Phys. Chem. C 2013, 117, 17382−17398

the injection evidently. However, Troisi and co-workers[24] also verified that another factor for the slower injection is the localization of the LUMO away from the carboxylic acid anchoring group; if the surface states available are not coupled strongly to the sensitizer, the injection will be slower than if the states available are coupled very largely. From Table 4, one can find that the proportion of the LUMO localized on the carboxylic acid group (Q_{LUMO}) of **DT**, **SDT**, and **CDT** families is smaller than that of **DQ**, **SDQ**, and **CDQ** families. Interestingly, the change tendency of the Q_{LUMO} in **DT**, **SDT**, and **CDT** sets is decreased in the order of −A1, −A4, −A, −A3, and −A2 featured dyes, while it decreased in the order of −A1, −A3, −A2, −A, and −A4 featured dyes in **DQ**, **SDQ**, and **CDQ** families. At the same time, the Q_{LUMO} of **SDT** and **SDQ** families is the largest in all considered systems, which displays stronger coupling with the semiconductor surface. As a result, the −A1 acceptor constructed sensitizers produce the largest Q_{LUMO} and compensate well the relative smaller injection energy E_s. On the other hand, if one considers the −A2 or −A3 acceptor capped chromophores, which inject at very similar E_s toward an almost identical density of TiO_2 acceptor states, it could infer that the charge injection into the TiO_2 surface of −A3 featured chromophores should be more rapid due to that they possess higher Q_{LUMO} than that of the −A2 constructed chromophores, and the difference of Q_{LUMO} between the −A2 and −A3 featured chromophores is more evident in **DQ**, **SDQ**, and **CDQ** sets as compared to **DT**, **SDT**, and **CDT** dyes. On the basis of the report by Troisi et al.,[24] a triphenylamine dye with 2-cyanoacrylic acid acceptor and an anthraquinone dye with the benzoic acid acceptor inject at very similar energies (−2.72 and −2.73 eV, respectively) toward an almost identical density of TiO_2 acceptor states; the rate differs by almost 2 orders of magnitude and the highest IPCE value of the latter one is only 3.9% at 540 nm, indicating that high E_s could not ensure a fast injection rate independently. Consequently, we infer that our considered systems that constructed the −A or −A1 acceptor combined with the quinoxaline auxiliary acceptor might produce the faster charge injection and higher IPCE.

3.4. Evaluating the Tendency of Charge Recombination. Commonly, the dyes after photoexcitation by solar radiation could inject an electron into the conduction band of TiO_2 very rapidly; however, the injected electron in the conduction band could recombine with the oxidized dye or the oxidized component in the redox pair, for instance, the redox couple (I^-/I^-_3) in the electrolyte, and the other factor such as the nonradiative deexcitation of the dye. Thus, evaluating the tendency of charge recombination is most critical, and the corresponding items[27,42] enter eqs 7−12 for dye−semiconductor coupling $\Gamma(E)$ and Franck−Condon term $F(E)$, respectively. The $\Gamma(E)$ in eq 8 is proportional to the semiconductor density of states $\rho_{kk'}$ and the semiconductor−dye coupling V_{mk}. Meanwhile, for evaluating the charge recombination, c_m presents the dye's HOMO coefficients (for evaluating the charge injection, c_m presents the dye's LUMO coefficients), which belonging to the anchoring (carboxylic) group contribute significantly to $\Gamma(E)$. In this section, we follow the same pattern with section 3.3 that reasonably assumes that the electrode density of states $\rho_{kk'}$ and semiconductor−dye coupling V_{mk} under our investigated systems would be almost identical in every dye−semiconductor system, and only the HOMO coefficients c_m will differ depending on the details of the dyes' structure. The frontier orbitals plot of every chromophore shows that the HOMO is mainly localized on the molecule's indoline core (not shown); as such, the weight of the HOMO on the carboxylic group (Q_{HOMO}) will differ depending on the details of the dye's conjunction length. On the basis of Figure 1, the whole length of molecular backbone in all families decreased in the order **CDT** ≈ **CDQ** > **SDT** ≈ **SDQ** > **DT** ≈ **DQ**, and is shortened in the order of −A4, −A3, −A2, −A1, and −A featured dyes in every set. As is seen from Table 5, the largest-to-smallest ordering of Q_{HOMO} in every family is the −A, −A1, −A2, −A3, and −A4 capped dyes, which is opposite of the decreased whole backbone length. On the other hand, substitution of the benzothiadiazole with quinoxaline as auxiliary acceptor, and introduction of electron-donating group could not improve the Q_{HOMO} to some extent. The above phenomenon indicates that as the length of whole backbone is shortened, the Q_{HOMO} is increased, while as the coplanar of the backbone is weakened, the Q_{HOMO} decreases. As such, the $\Gamma(E)$ is proportional to the Q_{HOMO} and decreased in the order **DT** > **SDT** > **DQ** > **CDT** > **SDQ** > **CDQ**. However, this sequence of $\Gamma(E)$ might not produce the correct ordering of the charge recombination independently due to the nuclear motion factor, and the relative energies of the neutral dye and its cation described by the Franck−Condon term F(E) in eq 11 could influence the charge recombination also. Therefore, we use the E_{CB} = −4.0 eV in ref 27 to fast predict $F(E)$ roughly. Accordingly, the terms of free energy change ΔG and reorganization energy λ are computed and tabulated in Table

Table 5. Free Energy Differences ΔG, Reorganization Energies λ, and the Weight of the HOMO on the Anchoring Group (Carboxylic) Q_{HOMO} of All Dyes

dyes	ΔG	λ	λ_h	λ_e	Q_{HOMO} (%)
WS-9	−5.00	0.48	0.20	0.28	0.42
DT-A1	−5.05	0.39	0.18	0.21	0.38
DT-A2	−4.89	0.45	0.21	0.24	0.19
DT-A3	−4.92	0.43	0.21	0.22	0.15
DT-A4	−4.99	0.41	0.19	0.22	0.15
DQ-A	−5.01	0.46	0.18	0.28	0.32
DQ-A1	−5.05	0.38	0.16	0.22	0.27
DQ-A2	−4.91	0.31	0.19	0.12	0.17
DQ-A3	−4.94	0.41	0.19	0.22	0.12
DQ-A4	−5.00	0.39	0.17	0.22	0.11
SDT-A	−4.94	0.46	0.18	0.28	0.36
SDT-A1	−4.98	0.39	0.17	0.22	0.34
SDT-A2	−4.84	0.44	0.20	0.24	0.16
SDT-A3	−4.87	0.42	0.19	0.23	0.12
SDT-A4	−4.93	0.39	0.17	0.22	0.13
SDQ-A	−4.94	0.45	0.17	0.28	0.26
SDQ-A1	−4.97	0.38	0.15	0.23	0.24
SDQ-A2	−4.86	0.41	0.17	0.24	0.13
SDQ-A3	−4.88	0.39	0.17	0.22	0.09
SDQ-A4	−4.94	0.38	0.16	0.22	0.09
CDT-A	−5.00	0.42	0.14	0.28	0.29
CDT-A1	−5.03	0.35	0.13	0.22	0.26
CDT-A2	−4.91	0.39	0.15	0.24	0.15
CDT-A3	−4.93	0.35	0.12	0.23	0.11
CDT-A4	−4.99	0.35	0.13	0.22	0.10
CDQ-A	−5.00	0.40	0.13	0.27	0.21
CDQ-A1	−5.02	0.33	0.12	0.21	0.18
CDQ-A2	−4.92	0.36	0.13	0.23	0.12
CDQ-A3	−4.94	0.35	0.13	0.22	0.08
CDQ-A4	−4.99	0.35	0.13	0.22	0.07

dx.doi.org/10.1021/jp402645h | J. Phys. Chem. C 2013, 117, 17382−17398

5. It is found that the cation form is most effectively stabilized in the −A2 or −A3 capped sensitizers in every family, and at the same time, the stabilized cation form is opposite of the change of free energy ΔG, which decreased in order of −A1, −A, −A4, −A3, and −A2 constructed dyes in every set. Moreover, the difference of ΔG is subtle between the quinoxaline and benzothiadiazole featured dyes, and decreased in the order of **DT** ≈ **DQ** > **CDT** ≈ **CDQ** > **SDT** ≈ **SDQ** families, respectively. On the other hand, the reorganization energy λ in eq 11 should not be negligible due to that its magnitude could influence the $F(E)$ as well. The data of λ in Table 5 contain the hole reorganization energy λ_h and electron reorganization energy λ_e; the smaller total λ value obtained from the slower recombination would be due to smaller total λ that favors the separation of hole-charge. It is noted that the introduction of electron-donating group, −A1 or −A4 acceptor, and quinoxaline auxiliary acceptor could show the smaller λ. As a whole, the order of decreased λ is **DT** > **SDT** > **CDT** > **DQ** > **SDQ** > **CDQ**, respectively. Therefore, on the basis of ΔG and λ, we infer that the $F(E)$ maximum for −A2 or −A3 featured **SDT** and **SDQ** dyes occurs closest to the CB; consequently, at the energies closest to the conduction band edge (i.e., the energies corresponding to the largest electron population in the conduction band according to the Fermi−Dirac distribution), the −A2 or −A3 featured **SDT** and **SDQ** dyes would render the largest values of $F(E)$, subsequently increasing the charge recombination potentially, and an opposite result should be observed in −A1 attached **DQ** and **CDQ** dyes. Thus, taking the influences of $\Gamma(E)$ and $F(E)$ into account, we predict that dyes **DQ-A1** and **CDQ-A1** should possess the relatively slower recombination rate.

3.5. Dipole Moment. An experimental study performed by Nazeeruddin et al.[64] and some reports via first-principles calculations[19,20,45] have pointed out that there is correlation between the dipole moment μ_{normal} of the adsorbed dyes and the energy shift of E_{CB} in liquid DSSC. Therefore, we propose a reasonable prediction based on the issue related to V_{oc}. According to eqs 13 and 14, it is obvious that a dye with a large μ_{normal} will induce a significant variation of V_{oc}. In this sense, we compute the μ_{normal} of all isolated dyes first to evaluate the change tendency roughly. Considering the bidentate binding mode of all dyes, we make the C_2 axis of the carboxylate in the dye parallel to the *x*-axis, and the semiconductor surface parallel to the *yz* plane (Figure 3a and b); the characterized data are tabulated in Table 6. One can find that the −A1 or −A4 acceptor capped dyes display a larger μ_{normal} as compared to other dyes in every family. Also, the fabrication of quinoxaline as auxiliary acceptor in **DQ**, **SDQ**, and **CDQ** families could induce a smaller μ_{normal} as compared to benzothiadiazole featured **DT**, **SDT**, and **CDT** sets. In addition to the influence of the acceptor and additional acceptor subunits on the μ_{normal}, the effect of electron-donating group could not be negligible. It is interesting to note that the introduction of alkyloxy chain in **SDT** and **SDQ** families could yield an enhanced μ_{normal}, while featuring the ethane-1,1-diyldibenzene moiety in **CDT** and **CDQ** sets could render a reverse result. Subsequently, we conclude that featuring −A1 or −A4 acceptor, benzothiadiazole auxiliary acceptor and alkyloxy chain in dyes could exhibit the prominent μ_{normal}, which is related to the large V_{oc} values potentially.

3.6. Fast Screening and Characterization of a Promising Candidate. On the basis of the initial calculated data above, we screen out that **CDQ-A1** and **CDQ-A4** would be the best candidates, the main reason being that their performance is optimized in terms of achieving a balance among competing factors (i.e., smaller lowest energy transition, higher light harvesting efficiency, moderate dipole moment, relative stronger coupling between the anchoring group and the TiO_2 surface, albeit a smaller injection energy) with respect to their counterpart **WS-9** for application in future DSSCs in our investigation.

Thus, exploration of the absorption of adsorbed system and the charge recombination mechanism of the injected electron in the conduction band with the redox couple (I^-/I_3^-) in the electrolyte is more critical for an excellent dye-sensitizer. Therefore, the characterization of UV−vis for **WS-9**, **CDQ-A1**, and **CDQ-A4** adsorbed on the TiO_2 surface is performed to investigate how the interfacial interaction between the dye and semiconductor influences the electron excitation. Currently, $Ti(OH)_3H_2O$[65,66] as a TiO_2 model could reasonably describe the electronic coupling interaction between organic dye and the semiconductor for the absorption, but it is necessary to use a

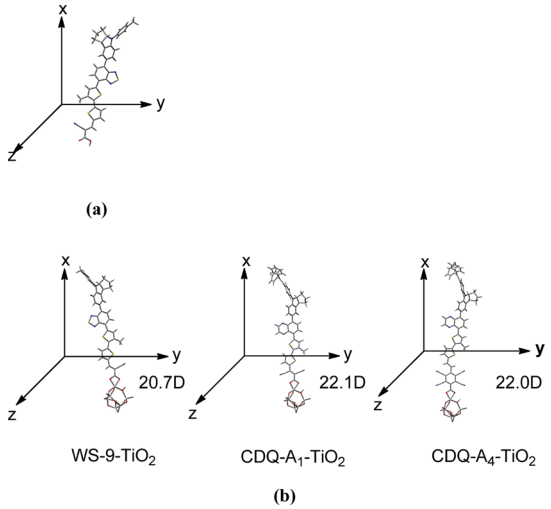

Figure 3. (a) Representation of coordinates for the calculation of normal dipole moment (μ_{normal}) of isolated dye. (b) Calculated vertical dipole moment of dyes **WS-9**, **CDQ-A1**, and **CDQ-A4** at $(TiO_2)_6$ cluster.

Table 6. Evaluated Dipole Moment μ_{normal} (Units in Debye)

dyes	μ_{normal}[a]	dyes	μ_{normal}[a]
WS-9	13.7	**DQ-A**	12.7
DT-A1	17.1	**DQ-A1**	16.0
DT-A2	12.2	**DQ-A2**	11.6
DT-A3	12.1	**DQ-A3**	11.4
DT-A4	17.8	**DQ-A4**	17.1
SDT-A	15.3	**SDQ-A**	14.4
SDT-A1	18.8	**SDQ-A1**	17.7
SDT-A2	13.7	**SDQ-A2**	13.2
SDT-A3	13.7	**SDQ-A3**	13.0
SDT-A4	19.5	**SDQ-A4**	18.7
CDT-A	12.3	**CDQ-A**	11.7
CDT-A1	15.3	**CDQ-A1**	14.5
CDT-A2	10.6	**CDQ-A2**	10.2
CDT-A3	10.9	**CDQ-A3**	10.3
CDT-A4	15.6	**CDQ-A4**	15.3

[a]The parameters are obtained by single point calculations in CH_2Cl_2 solution after geometry optimization.

dx.doi.org/10.1021/jp402645h | J. Phys. Chem. C 2013, 117, 17382−17398

more realistic TiO_2 model to accurately describe the electron excitation process and the charge redistribution of TiO_2 upon excitation. Thus, the model of $(TiO_2)_6$ cluster[66] is used to simulate the absorption (Figure 4a), and the electron density differences maps (EDDMs)[53] of dyes **WS-9**, **CDQ-A1**, and **CDQ-A4** before and after they bind on $(TiO_2)_6$ cluster are depicted in Figure 4b. As illustrated in Figure 4a, the maximum absorption peak of **WS-9**, **CDQ-A1**, and **CDQ-A4** after they adsorbed is red-shifted by ~39, ~67, and ~64 nm, respectively, which are assigned to the increased delocalization of the π^* orbital of the conjugated framework, evidenced by the interaction between the carboxylate group and the Ti^{4+} ions, which directly decreases the energy of the π^* level. The corresponding second-order perturbation energy $E^{(2)}$ in Supporting Information Table S5 suggests that upon the three dyes adsorbed on TiO_2 surface, the $E^{(2)}$ values are all decreased, giving an explanation to the increased delocalization of the π^* orbital indirectly. Furthermore, the oscillator strength f of the three after being adsorbed is improved further, which subsequently improves the LHE by 0.98%, 0.70%, and 0.20% that of the adsorbed for **WS-9**, **CDQ-A1**, and **CDQ-A4**, respectively, confirming that the coupling between these chromophores and TiO_2 surface is strong. In addition, the EDDM (Figure 4b) of isolated **WS-9** shows that the decreasing electron density (green) mainly localizes on the indoline and benzothiadiazole, and the increasing electron density (purple) mainly localizes on the benzothiadiazole and conjugation spacer with a slight weight on the acceptor/anchoring segment. On the contrary, the decreasing electron density mainly localizes on the electron-donating part, auxiliary acceptor, and the conjugation spacer, while the increasing electron density mainly delocalizes on the conjugation spacer and acceptor/anchoring group in **CDQ-A1** and **CDQ-A4**, which is indicative of a more evident electron separation in intramolecular charge transfer when the transition occurs as compared to **WS-9**. After binding, the EDDMs of the three dyes all demonstrate an evident charge migration from the donor part to $(TiO_2)_6$ when transition occurs. To be more quantitative, the NBO analysis of the atomic charge redistributions of $(TiO_2)_6$ in the ground state (S_0) and excited state (S_1) extracted is carried out to provide initial evidence to illustrate the process of photoinduced electron. The result in Table 7 demonstrates that the number of photoinduced electron n_c in $(TiO_2)_6$ from the S_0 to S_1 state for both **CDQ-A1** and **CDQ-A4** is larger than that of **WS-9**. Besides, the μ_{normal} and the shift of conduction band edge ΔE_{CB} after being adsorbed would also be evidence to predict the V_{oc} unambiguously. As is seen from Figure 3b, the larger μ_{normal} is found in **CDQ-A1** (22.1 D) ≈ **CDQ-A4** (22.0 D) with respect to **WS-9** (20.7 D), and the larger ΔE_{CB} values of **CDQ-A1** (0.23 eV) and **CDQ-A4** (0.26 eV) are revealed as compared to that of **WS-9** (0.12 eV) in Supporting Information Figure S4. As such, based on eq 13, the larger n_c, μ_{normal}, and ΔE_{CB} of **CDQ-A1** and **CDQ-A4** should enhance the V_{oc} potentially as

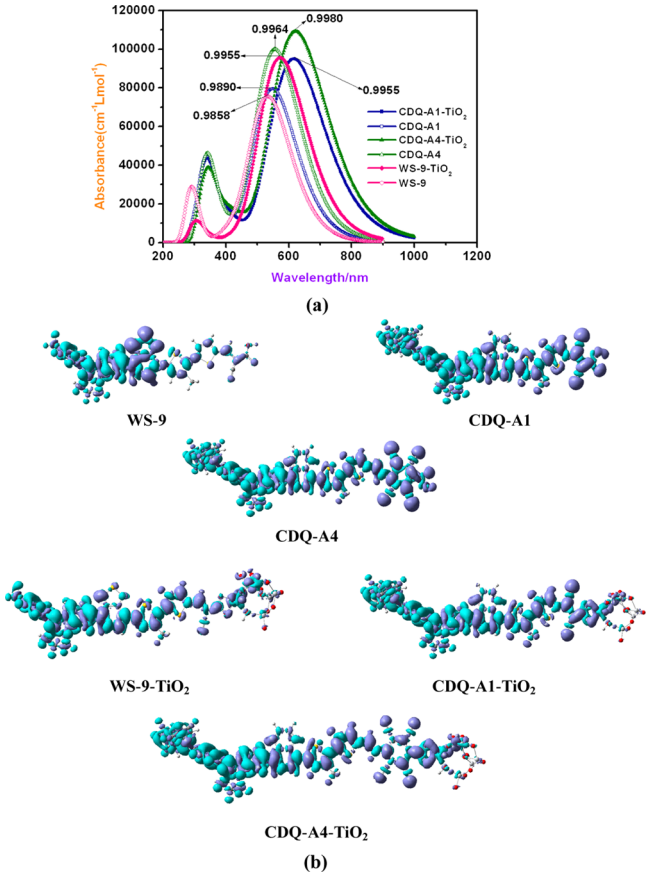

Figure 4. (a) The UV−vis spectra of **WS-9**, **CDQ-A1**, and **CDQ-A4** binding on TiO_2 surface in CH_2Cl_2 solution. (b) The electron density differences maps (EDDMs) of dyes **WS-9**, **CDQ-A1**, and **CDQ-A4** before and after binding on TiO_2 film between the ground state and the first excited state are simulated by Multiwfn 3.0.1 (the purple represents where the electrons are coming from, and the green represents where the electrons are going).

Table 7. Absorption Spectra and $(TiO_2)_6$ Atomic Charge Distribution (in au) of the Ground State (S_0) and Excited State (S_1) of the WS-9, CDQ-A1, and CDQ-A4 after They Bind on TiO_2 Surface

	absorption data				atomic charge distribution (au)		
dyes−TiO_2	energy/eV	transition nature	f	λ_{max}/nm	S_0	S_1	Δq^a
WS-9	2.16(S_0→S_1)	H→L(29.0%)	2.3509	573.3	0.317	0.315	0.002
	2.78(S_0→S_2)	H→L+3(39.8%)	0.1156	445.9			
	4.11(S_0→S_9)	H→L+15(17.4%)	0.1903	301.7			
CDQ-A1	2.01(S_0→S_1)	H→L(41.3%)	2.3433	616.5	0.332	0.328	0.004
	3.05(S_0→S_3)	H→L+4(58.4%)	0.3304	406.8			
	3.65(S_0→S_5)	H→L+16(47.3%)	0.6150	339.5			
CDQ-A4	1.99(S_0→S_1)	H−1→L(48.7%)	2.6944	622.0	0.464	0.375	0.089
	2.96(S_0→S_4)	H→L+5(35.5%)	0.3281	419.2			
	3.66(S_0→S_8)	H→L+3(15.9%)	0.4191	338.7			

[a] Δq is the charge differences on TiO_2 surface between S_0 and S_1.

dx.doi.org/10.1021/jp402645h | J. Phys. Chem. C 2013, 117, 17382−17398

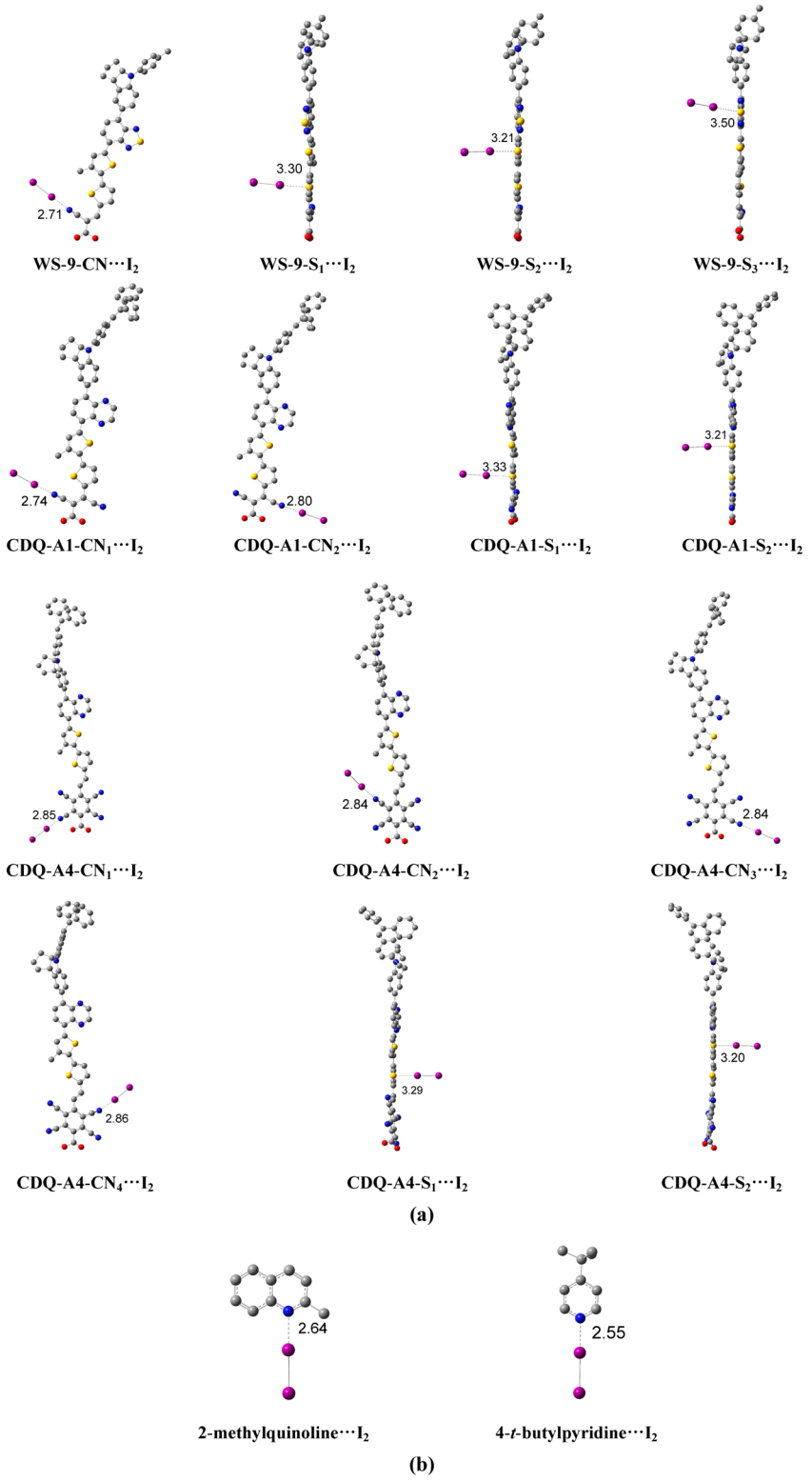

Figure 5. (a) Optimized molecular distances of the dye···I_2 complexes. (b) Distances of the two additive···I_2 complexes (units in Å).

compared to **WS-9**. However, these items could not guarantee a high V_{oc} individually because the injected electron in the conduction band of the semiconductor could recombine with the redox couple (I^-/I^-_3) in the electrolyte as well as the oxidized organic dyes, and the former one is the main route of photovoltage losses.[34] The accepted knowledge is that the higher is the iodine concentration close to the TiO_2 surface, the shorter is the electron lifetime in the CB, which is related to lower V_{oc} values. Hence, to reveal the reason of the interfacial charge recombination, we simulate the interaction between the three dyes and electron acceptor in electrolyte further. The optimized geometries of the dye···I_2 complexes under the B3LYP/6-31G* (LANL2DZ basis set for I atom) level in gas phase are plotted in Figure 5a. It is apparent that I_2 preferred

dx.doi.org/10.1021/jp402645h | J. Phys. Chem. C 2013, 117, 17382−17398

binding three sites for **WS-9**, **CDQ-A1**, and **CDQ-A4** are found to be at N of CN, S of thiophene, and S of benzothiadiazole forming the halogen bonding[67] through a noncovalent interaction. For each dye, the S atoms are labeled as S1, S2, and S3 in turn from the acceptor toward the donor part, and the distances of I_2 with different electron donor sites on these molecules are then calculated to determine the preferred binding site. On the basis of our calculations, the lengthened intramolecular I−I bond lengths in all complexes are larger than the covalent radii 2.86 Å (not shown), indicating that the I_2 monomer bond is weakened. At the same time, the distances of the first preferred binding site at CN group (CN···I_2) are smaller than the net van der Waals radii 3.53 Å of the binding atoms, but larger than the net covalent radii 2.03 Å.[34] In addition, a similar result is also detected in the distances of S···I_2, which is stronger than the net van der Waals radii 3.78 Å[67] and weaker than the net covalent radii. Furthermore, it is noted that the distances of noncovalent interaction of dye···I_2 complexes of **CDQ-A1** and **CDQ-A4** are both larger than that of **WS-9** in the same electron-donating position, revealing that the intermolecular interaction between **CDQ-A1** and **CDQ-A4** with I_2 is weaker as compared to **WS-9**. Typically, to reduce the electron losses, one method is to add organic compounds to the electrolyte, such as nitrogen-containing heterocycles (example as 4-*t*-butylpyridine), which have been proved to drastically enhance both the V_{oc} and the η finally.[34] On the basis of the finding, the interaction between additives (**4**-*t*-butylpyridine and 2-methylquinoline) with iodine is reproduced. The optimized adducts are plotted in Figure 5b. The distances of additive···I_2 adducts are both smaller than that of the dye···I_2 complexes, suggesting that the intermolecular interaction in additive···I_2 adducts is stronger, and, as a result, diminishes the iodine concentration close to the TiO_2 surface. On the other hand, to account for the reason for electron recombination, the NBO analysis is conducted in CH_2Cl_2 solution unambiguously, and the corresponding result is presented in Table 8. The negative atomic charge distributions of I_2 in different electron-donating sites of dye **CDQ-A1** and **CDQ-A4** are larger as compared to **WS-9**, showing that the electron recombination would be weakened in **CDQ-A1** and **CDQ-A4** due to their larger size and the absent of the S atom in quinoxaline subunit. Furthermore, our computed result displays that the negative atomic charge of I_2 in additive···I_2 adducts is smaller than that of dye···I_2 complexes, supporting that these two additives would lead to a stronger intermolecular charge-transfer where merited to the longer electron lifetime in the conduction band. Table 8 also shows the formed interaction of dye···I_2 complexes via lone pair (LP) → antibond (σ^*) where the LP N or LP S participates as an electron donor and the σ^* I−I antibond as an electron acceptor in the intermolecular charge-transfer interaction. The N atom interacts with I_2 using one valence lone pair, LP (1) N, while the S atom possesses two valence lone pairs, LP (1) S and LP (2) S. The interaction of LP → σ^* I−I can be considered as a measure of the relative stability of adduct, the larger $E^{(2)}$ values of LP → σ^* I−I indicate the interaction is more stable, and, subsequently, the electron loss is more serious. One can note that the $E^{(2)}$ values of different electron-donating positions in **CDQ-A1** and **CDQ-A4** are all smaller than that of **WS-9**, confirming that the interaction between **WS-9** and iodine is more stable as compared to **CDQ-A1** and **CDQ-A4**; as such, the photovoltage loss is more serious. On the other hand, **2**-methylquinoline and **4**-*t*-butylpyridine as additives present a larger $E^{(2)}$ value as compared to dyes **WS-9**, **CDQ-A1**, and **CDQ-A4**, elucidating the vital function of additive in electrolyte essentially. These results are in well accordance with the distance change tendency and the atomic charge distributions.

Table 8. Calculated Iodide Atomic Charge (au) on the Iodine of Various Adducts and Second-Order Perturbation Energy ($E^{(2)}$, kcal mol^{-1})

complexes	iodide atomic charge (au)		$E^{(2)}$ (kcal mol^{-1})
WS-9-CN···I_2	−0.101	LP (1) N→σ^* I−I	18.34
WS-9-S_1···I_2	−0.192	LP (1) S1→σ^* I−I	1.40
		LP (2) S1→σ^* I−I	12.92
WS-9-S_2···I_2	−0.205	LP (1) S2→σ^* I−I	2.08
		LP (2) S2→σ^* I−I	17.96
WS-9-S_3···I_2	−0.200	LP (1) S3→σ^* I−I	1.15
		LP (2) S3→σ^* I−I	5.15
CDQ-A1-CN_1···I_2	−0.091	LP (1) N1→σ^* I−I	16.66
CDQ-A1-CN_2···I_2	−0.075	LP (1) N2→σ^* I−I	13.27
CDQ-A1-S_1···I_2	−0.177	LP (1) S1→σ^* I−I	1.31
		LP (2) S1→σ^* I−I	11.39
CDQ-A1-S_2···I_2	−0.194	LP (1) S2→σ^* I−I	2.13
		LP (2) S2→σ^* I−I	17.52
CDQ-A4-CN_1···I_2	−0.063	LP (1) N1→σ^* I−I	11.03
CDQ-A4-CN_2···I_2	−0.066	LP (1) N2→σ^* I−I	11.62
CDQ-A4-CN_3···I_2	−0.066	LP (1) N3→σ^* I−I	11.50
CDQ-A4-CN_4···I_2	−0.060	LP (1) N4→σ^* I−I	10.50
CDQ-A4-S_1···I_2	−0.196	LP (1) S1→σ^* I−I	1.56
		LP (2) S1→σ^* I−I	13.55
CDQ-A4-S_2···I_2	−0.108	LP (1) S2→σ^* I−I	2.09
		LP (2) S2→σ^* I−I	18.48
4-*t*-butylpyridine···I_2	−0.268	LP (1) N→σ^* I−I	36.17
2-methylquinoline···I_2	−0.270	LP (1) N→σ^* I−I	42.33

As a whole, taking the competing factors into account, we screen out **CDQ-A1** as the most promising candidate among these newly designed organic dye-sensitizers under our investigation due to it not only possessing the longer absorption wavelength, larger LHE value, μ_{normal}, but it also owns less electron-donating sites with redox couple in the electrolyte, which merits less electron loss. Table 9 summarizes the performances of dye **WS-9** sensitized DSSCs in the different conditions.[9] Following the J_{sc}, V_{oc}, and η values, we could expect that the DSSC using dye **CDQ-A1** in the optimized condition should exert an excellent J_{sc} and V_{oc} with respect to **WS-9**, and the overall energy conversion efficiency η would be improved and exceed over 9.02%.

Table 9. Photovoltaic Characteristics[a] for DSSCs Based on WS-9 Using CH_2Cl_2 as Sensitizing Bath Solvent

WS-9	J_{sc}/mA cm^{-2}	V_{oc}/mV	*ff*	η/%
0 mM CDCA[b]	17.26	692	0.64	7.63
20 mM CDCA[b]	18.15	702	0.71	9.02

[a]Experimental values are from ref 9. [b]Coadsorbent (chenodeoxycholic acid).

4. CONCLUSION

In summary, a series of indoline-based organic dyes have been designed and characterized theoretically. By modifications on

dx.doi.org/10.1021/jp402645h | J. Phys. Chem. C 2013, 117, 17382−17398

the electron-donating moiety, auxiliary acceptor, and acceptor fragments while artificially fixing the π bridge, we successfully screen out dye **CDQ-A1** as the best candidate due to that it performs nicely on the parameters of maximum absorption λ_{max}, light harvesting efficiency LHE, adsorbed dipole moment, kinetics of electron injection, and recombination could achieve a good balance, which are superior to those of **WS-9**. We hope this will be helpful for the design of organic dye with target properties to improve the performance of DSSCs. Further optimization of photovoltaic performance, including the modification on molecular structure and exploration of the relationship between structure and properties, is still in progress.

■ ASSOCIATED CONTENT

Supporting Information

Table S1: Critical dihedral angles. Table S2: Atomic charge distribution. Table S3: Calculated relative LHE. Table S4: Second transition dipole moment. Table S5: Calculated second-order perturbation energy. Figure S1: DOSs and PDOSs. Figure S2: Optimized distances. Figure S3: Frontier molecular energy levels. Figure S4: DOSs and PDOSs on $(TiO_2)_6$ clusters. This material is available free of charge via the Internet at http://pubs.acs.org.

■ AUTHOR INFORMATION

Corresponding Author

*Tel.: +86-931-7971989. Fax: +86-931-7971989. E-mail: zhiyuangeng@126.com.

Notes

The authors declare no competing financial interest.

■ ACKNOWLEDGMENTS

We thank the Natural Science Foundation of Gansu province (Grant No. 10710RJZA114), the Natural Science Foundation of Gansu province education office (Grant No. 10801-10), and the Gansu Supercomputer Center.

■ REFERENCES

(1) Yella, A.; Lee, H.-W.; Tsao, H. N.; Yi, C.; Chandiran, A. K.; Nazeeruddin, M. K.; Diau, E. W.-G.; Yeh, C.-Y.; Zakeeruddin, S. M.; Grätzel, M. Porphyrin-Sensitized Solar Cells with Cobalt (II/III)-Based Redox Electrolyte Exceed 12% Efficiency. *Science* **2011**, *334*, 629−634.

(2) Burschka, J.; Pellet, N.; Moon, S.-J.; Humphry-Baker, R.; Gao, P.; Nazeeruddin, M. K.; Grätzel, M. Sequential Deposition as a Route to High-Performance Perovskite-Sensitized Solar Cells. *Nature* **2013**, *499*, 316−319.

(3) Shalom, M.; Buhbut, S.; Tirosh, S.; Zaban, A. Design Rules for High-Efficiency Quantum-Dot-Sensitized Solar Cells: A Multilayer Approach. *J. Phys. Chem. Lett.* **2012**, *3*, 2436−2441.

(4) O'Regan, B. C.; Grätzel, M. A Low-Cost, High-Efficiency Solar Cell Based on Dye-Sensitized Colloidal TiO_2 Films. *Nature* **1991**, *353*, 737−740.

(5) Nazeeruddin, M. K.; De Angelis, F.; Fantacci, S.; Selloni, A.; Viscardi, G.; Liska, P.; Ito, S.; Takeru, B.; Grätzel, M. Combined Experimental and DFT-TDDFT Computational Study of Photoelectrochemical Cell Ruthenium Sensitizers. *J. Am. Chem. Soc.* **2005**, *127*, 16835−16847.

(6) Zeng, W.; Cao, Y.; Bai, Y.; Wang, Y.; Shi, Y.; Zhang, M.; Wang, F.; Pan, C.; Wang, P. Efficient Dye-Sensitized Solar Cells with an Organic Photosensitizer Featuring Orderly Conjugated Ethylenedioxythiophene and Dithienosilole Blocks. *Chem. Mater.* **2010**, *22*, 1915−1925.

(7) Bai, Y.; Zhang, J.; Zhou, D.; Wang, Y.; Zhang, M.; Wang, P. Engineering Organic Sensitizers for Iodine-Free Dye-Sensitized Solar Cells: Red-Shifted Current Response Concomitant with Attenuated Charge Recombination. *J. Am. Chem. Soc.* **2011**, *133*, 11442−11445.

(8) Yang, J.; Guo, F.; Hua, J.; Li, X.; Wu, W.; Qu, Y.; Tian, H. Efficient and Stable Organic DSSC Sensitizers Bearing Quinacridone and Furan Moieties as a Planar π-Spacer. *J. Mater. Chem.* **2012**, *22*, 24356−24365.

(9) Wu, Y.; Marszalek, M.; Zakeeruddin, S. M.; Zhang, Q.; Tian, H.; Grätzel, M.; Zhu, W. High-Conversion-Efficiency Organic Dye-Sensitized Solar Cells: Molecular Engineering on D-A-π-A Featured Organic Indoline Dyes. *Energy Environ. Sci.* **2012**, *5*, 8261−8272.

(10) Ying, W.; Guo, F.; Li, J.; Zhang, Q.; Wu, W.; Tian, H.; Hua, J. Series of New D-A-π-A Organic Broadly Absorbing Sensitizers Containing Isoindigo Unit for Highly Efficient Dye-Sensitized Solar Cells. *ACS Appl. Mater. Interfaces* **2012**, *4*, 4215−24.

(11) Chang, Y. J.; Chou, P.-T.; Lin, Y.-Z.; Watanabe, M.; Yang, C.-J.; Chin, T.-M.; Chow, T. J. Organic Dyes Containing Oligo-Phenothiazine for Dye-Sensitized Solar Cells. *J. Mater. Chem.* **2012**, *22*, 21704−21712.

(12) Shi, J.; Chen, J.; Chai, Z.; Wang, H.; Tang, R.; Fan, K.; Wu, M.; Han, H.; Qin, J.; Peng, T.; et al. High Performance Organic Sensitizers Based on 11,12-Bis(Hexyloxy) Dibenzo [a,c]Phenazine for Dye-Sensitized Solar Cells. *J. Mater. Chem.* **2012**, *22*, 18830−18838.

(13) Feng, Q.; Lu, X.; Zhou, G.; Wang, Z.-S. Synthesis and Photovoltaic Properties of Organic Sensitizers Incorporating a Thieno[3,4-c]Pyrrole-4,6-Dione Moiety. *Phys. Chem. Chem. Phys.* **2012**, *14*, 7993−7999.

(14) Lu, X.; Feng, Q.; Lan, T.; Zhou, G.; Wang, Z.-S. Molecular Engineering of Quinoxaline-Based Organic Sensitizers for Highly Efficient and Stable Dye-Sensitized Solar Cells. *Chem. Mater.* **2012**, *24*, 3179−3187.

(15) Ren, X.; Jiang, S.; Cha, M.; Zhou, G.; Wang, Z.-S. Thiophene-Bridged Double D-π-A Dye for Efficient Dye-Sensitized Solar Cell. *Chem. Mater.* **2012**, *24*, 3493−3499.

(16) Zhang, X.; Liu, F.; Huang, Q.-L.; Zhou, G.; Wang, Z.-S. Dye-Sensitized W-Doped TiO_2 Solar Cells with a Tunable Conduction Band and Suppressed Charge Recombination. *J. Phys. Chem. C* **2011**, *115*, 12665−12671.

(17) Ambrosio, F.; Martsinovich, N.; Troisi, A. What Is the Best Anchoring Group for a Dye in a Dye-Sensitized Solar Cell? *J. Phys. Chem. Lett.* **2012**, *3*, 1531−1535.

(18) Zhang, J.; Li, H.-B.; Geng, Y.; Wen, S.-H.; Zhong, R.-L.; Wu, Y.; Fu, Q.; Su, Z.-M. Modification on C219 by Coumarin Donor toward Efficient Sensitizer for Dye Sensitized Solar Cells: A Theoretical Study. *Dyes Pigm.* **2013**, *99*, 127−135.

(19) Zhang, J.; Li, H.-B.; Sun, S.-L.; Geng, Y.; Wu, Y.; Su, Z.-M. Density Functional Theory Characterization and Design of High-Performance Diarylamine-fluorene Dyes with Different π Spacers for Dye-Sensitized Solar Cells. *J. Mater. Chem.* **2012**, *22*, 568−576.

(20) Zhang, J.; Kan, Y.-H.; Li, H.-B.; Geng, Y.; Wu, Y.; Su, Z.-M. How to Design Proper π-Spacer Order of The D−π−A Dyes for DSSCs? A Density Functional Response. *Dyes Pigm.* **2012**, *95*, 313−321.

(21) Namuangruk, S.; Fukuda, R.; Ehara, M.; Meeprasert, J.; Khanasa, T.; Morada, S.; Kaewin, T.; Jungsuttiwong, S.; Sudyoadsuk, T.; Promarak, V. D-D-π-A-Type Organic Dyes for Dye-Sensitized Solar Cells with a Potential for Direct Electron Injection and a High Extinction Coefficient: Synthesis, Characterization, and Theoretical Investigation. *J. Phys. Chem. C* **2012**, *116*, 25653−25663.

(22) Meng, S.; Kaxiras, E.; Nazeeruddin, M. K.; Grätzel, M. Design of Dye Acceptors for Photovoltaics from First-Principles Calculations. *J. Phys. Chem. C* **2011**, *115*, 9276−9282.

(23) Katono, M.; Bessho, T.; Wielopolski, M.; Marszalek, M.; Moser, J.-E.; Humphry-Baker, R.; Zakeeruddin, S. M.; Grätzel, M. Influence of the Anchoring Modes on the Electronic and Photovoltaic Properties of D-π-A Dyes. *J. Phys. Chem. C* **2012**, *116*, 16876−16884.

(24) Jones, D. R.; Troisi, A. A Method to Rapidly Predict the Charge Injection Rate in Dye Sensitized Solar Cells. *Phys. Chem. Chem. Phys.* **2010**, *12*, 4625−4634.
(25) Thapa, R.; Park, N. First-Principles Identification of Iodine Exchange Mechanism in Iodide Ionic liquid. *J. Phys. Chem. Lett.* **2012**, *3*, 3065−3069.
(26) Richards, C. E.; Anderson, A. Y.; Martiniani, S.; Law, C.; O'Regan, B. C. The Mechanism of Iodine Reduction by TiO_2 Electrons and the Kinetics of Recombination in Dye-Sensitized Solar Cells. *J. Phys. Chem. Lett.* **2012**, *3*, 1980−1984.
(27) Maggio, E.; Martsinovich, N.; Troisi, A. Evaluating Charge Recombination Rate in Dye-Sensitized Solar Cells from Electronic Structure Calculations. *J. Phys. Chem. C* **2012**, *116*, 7638−7649.
(28) Long, R.; English, N. J.; Prezhdo, O. V. Photo-Induced Charge Separation Across the Graphene-TiO_2 Interface is Faster Than Energy Losses: A Time-Domain ab initio Analysis. *J. Am. Chem. Soc.* **2012**, *134*, 14238−14248.
(29) Hoff, D. A.; Da Silva, R.; Rego, L. G. C. Coupled Electron−Hole Quantum Dynamics on D-π-A Dye-Sensitized TiO_2 Semiconductors. *J. Phys. Chem. C* **2012**, *116*, 21169−21178.
(30) Zhang, J.; Hughes, T. F.; Steigerwald, M.; Brus, L.; Friesner, R. A. Realistic Cluster Modeling of Electron Transport and Trapping in Solvated TiO_2 Nanoparticles. *J. Am. Chem. Soc.* **2012**, *134*, 12028−12042.
(31) Jungsuttiwong, S.; Tarsang, R.; Sudyoadsuk, T.; Promarak, V.; Khongpracha, P.; Namuangruk, S. Theoretical Study on Novel Double Donor-Based Dyes Used in High Efficient Dye-Sensitized Solar Cells: the Application of TDDFT Study to the Electron Injection Process. *Org. Electron.* **2013**, *14*, 711−722.
(32) Pastore, M.; Mosconi, E.; De Angelis, F. Computational Investigation of Dye−Iodine Interactions in Organic Dye-Sensitized Solar Cells. *J. Phys. Chem. C* **2012**, *116*, 5965−5973.
(33) Asaduzzaman, A. M.; Chappellaz, G. A. G.; Schreckenbach, G. Relationship between Dye−Iodine Binding and Cell Voltage in Dye-Sensitized Solar Cells: A Quantum-Mechanical Look. *J. Comput. Chem.* **2012**, *33*, 2492−2497.
(34) Kusama, H.; Sugihara, H. Theoretical Study of Quinolines−I_2 Intermolecular Interaction and Implications on Dye-Sensitized Solar Cell Performance. *J. Comput. Chem.* **2005**, *26*, 1372−1382.
(35) Kusama, H.; Sayama, K. Theoretical Study on the Intermolecular Interactions of Black Dye Dimers and Black Dye−Deoxycholic Acid Complexes in Dye-Sensitized Solar Cells. *J. Phys. Chem. C* **2012**, *116*, 23906−23914.
(36) Narayan, M. Review: Dye Sensitized Solar Cells Based on Natural Photosensitizers. *Renewable Sustainable Energy Rev.* **2012**, *16*, 208−215.
(37) Nalwa, H. S. *Handbook of Advanced Electronic and Photonic Materials and Devices*; Academic Press: San Diego, CA, 2001.
(38) Katoh, R.; Furube, A.; Yoshihara, T.; Hara, K.; Fujihashi, G.; Takano, S.; Murata, S.; Arakawa, H.; Tachiya, M. Efficiencies of Electron Injection from Excited N3 Dye into Nanocrystalline Semiconductor (ZrO_2, TiO_2, ZnO, Nb_2O_5, SnO_2, In_2O_3) Films. *J. Phys. Chem. B* **2004**, *108*, 4818−4822.
(39) Sang-aroon, W.; Saekow, S.; Amornkitbamrung, V. Density Functional Theory Study on the Electronic Structure of Monascus Dyes as Photosensitizer for Dye-Sensitized Solar Cells. *J. Photochem. Photobiol., A* **2012**, *236*, 35−40.
(40) Chen, S.-L.; Yang, L.-N.; Li, Z.-S. How to Design More Efficient Organic Dyes for Dye-Sensitized Solar Cells? Adding More sp^2-Hybridized Nitrogen in the Triphenylamine Donor. *J. Power Sources* **2013**, *223*, 86−93.
(41) Yang, L.-N.; Sun, Z.-Z.; Chen, S.-L.; Li, Z.-S. The Effects of Various Anchoring Groups on Optical and Electronic Properties of Dyes in Dye-Sensitized Solar Cells. *Dyes Pigm.* **2013**, *99*, 29−35.
(42) Maggio, E.; Martsinovich, N.; Troisi, A. Using Orbital Symmetry to Minimize Charge Recombination in Dye-Sensitized Solar Cells. *Angew. Chem., Int. Ed.* **2013**, *52*, 973−975.
(43) Martsinovich, N.; Troisi, A. Theoretical Studies of Dye-Sensitised Solar Cells: From Electronic Structure to Elementary Processes. *Energy Environ. Sci.* **2011**, *4*, 4473−4495.
(44) Balanay, M. P.; Kim, D. H. Structures and Excitation Energies of Zn−Tetraarylporphyrin Analogues: A Theoretical Study. *J. Mol. Struct. (THEOCHEM)* **2009**, *910*, 20−26.
(45) Feng, J.; Jiao, Y.; Ma, W.; Nazeeruddin, M. K.; Grätzel, M.; Meng, S. First Principles Design of Dye Molecules with Ullazine Donor for Dye Sensitized Solar Cells. *J. Phys. Chem. C* **2013**, *117*, 3772−3778.
(46) Foster, J. P.; Weinhold, F. Natural Hybrid Orbitals. *J. Am. Chem. Soc.* **1980**, *102*, 7211−7218.
(47) Frisch, M. J.; Trucks, G. W.; Schlegel, H. B.; Scuseria, G. E.; Robb, M. A.; Cheeseman, J. R.; Scalmani, G.; Barone, V.; Mennucci, B.; Petersson, G. A.; et al. *Gaussian 09*, revision A.02; Gaussian, Inc.: Wallingford, CT, 2009.
(48) Becke, A. D. Density-Functional Thermochemistry. III. The Role of Exact Exchange. *J. Chem. Phys.* **1993**, *98*, 5648−5652.
(49) Becke, A. D. A New Mixing of Hartree Fock and Local Density Functional Theories. *J. Chem. Phys.* **1993**, *98*, 1372.
(50) Cossi, M.; Rega, N.; Scalmani, G.; Barone, V. Energies, Structures, and Electronic Properties of Molecules in Solution with the C-PCM Solvation Model. *J. Comput. Chem.* **2003**, *24*, 669−681.
(51) Yanai, T.; Tew, D.; Handy, N. A New Hybrid Exchange-Correlation Functional Using the Coulomb-Attenuating Method (CAM-B3LYP). *Chem. Phys. Lett.* **2004**, *393*, 51−57.
(52) Lu, T.; Chen, F. W. Multiwfn: A Multifunctional Wavefunction Analyzer. *J. Comput. Chem.* **2012**, *33*, 580−592.
(53) Lu, T. *Multiwfn, Version 3.0.1, A Multifunctional Wavefunction Analyzer*; 2013; available at http://multiwfn.codeplex.com.
(54) Yao, B.-Q.; Sun, J.-S.; Tian, Z.-F.; Ren, X.-M.; Gu, D.-W.; Shen, L.-J.; Xie, J. Ion-Pair Charge Transfer Complexes with Intense Near IR Absorption: Syntheses, Crystal Structures, Electronic Spectra and DFT Calculations. *Polyhedron* **2008**, *27*, 2833−2844.
(55) Ding, W.-L.; Wang, D.-M.; Geng, Z.-Y.; Zhao, X.-L.; Xu, W.-B. Density Functional Theory Characterization and Verification of High-Performance Indoline Dyes with D-A-π-A Architecture for Dye-Sensitized Solar Cells. *Dyes Pigm.* **2013**, *98*, 125−135.
(56) Snaith, H. J. Estimating the Maximum Attainable Efficiency in Dye-Sensitized Solar Cells. *Adv. Funct. Mater.* **2010**, *20*, 13−19.
(57) Li, W.; Wu, Y.; Zhang, Q.; Tian, H.; Zhu, W. D-A-π-A Featured Sensitizers Bearing Phthalimide and Benzotriazole as Auxiliary Acceptor: Effect on Absorption and Charge Recombination Dynamics in Dye-Sensitized Solar Cells. *ACS Appl. Mater. Interfaces* **2012**, *4*, 1822−1830.
(58) Zhu, W.; Wu, Y.; Wang, S.; Li, W.; Li, X.; Chen, J.; Wang, Z.-S.; Tian, H. Organic D-A-π-A Solar Cell Sensitizers with Improved Stability and Spectral Response. *Adv. Funct. Mater.* **2011**, *21*, 756−763.
(59) Wu, Y.; Zhang, X.; Li, W.; Wang, Z.-S.; Tian, H.; Zhu, W. Hexylthiophene-Featured D−A−π−A Structural Indoline Chromophores for Coadsorbent-Free and Panchromatic Dye-Sensitized Solar Cells. *Adv. Energy Mater.* **2012**, *2*, 149−156.
(60) Cui, Y.; Wu, Y.; Lu, X.; Zhang, X.; Zhou, G.; Miapeh, F. B.; Zhu, W.; Wang, Z.-S. Incorporating Benzotriazole Moiety to Construct D−A−π−A Organic Sensitizers for Solar Cells: Significant Enhancement of Open-Circuit Photovoltage with Long Alkyl Group. *Chem. Mater.* **2011**, *23*, 4394−4401.
(61) Pei, K.; Wu, Y.; Islam, A.; Zhang, Q.; Han, L.; Tian, H.; Zhu, W. Constructing High-Efficiency D−A−π−A-Featured Solar Cell Sensitizers: A Promising Building Block of 2,3-Diphenylquinoxaline for Antiaggregation and Photostability. *ACS Appl. Mater. Interfaces* **2013**, *5*, 4986−4995.
(62) Preat, J.; Jacquemin, D.; Michaux, C.; Perpète, E. A. Improvement of the Efficiency of Thiophene-Bridged Compounds for Dye-Sensitized Solar Cells. *Chem. Phys.* **2010**, *376*, 56−68.
(63) Horiuchi, T.; Miura, H.; Sumioka, K.; Uchida, S. High Efficiency of Dye-Sensitized Solar Cells Based on Metal-Free Indoline Dyes. *J. Am. Chem. Soc.* **2004**, *126*, 12218−12219.

(64) Chen, P.; Yum, J. H.; De Angelis, F.; Mosconi, E.; Fantacci, S.; Moon, S.-J.; Humphry Baker, R.; Ko, J.; Nazeeruddin, M. K.; Grätzel, M. High Open-Circuit Voltage Solid-State Dye-Sensitized Solar Cells with Organic Dye. *Nano Lett.* **2009**, *6*, 2487−2492.
(65) Sánchez-de-Armas, R.; López, J. O.; San-Miguel, M. A.; Sanz, J. F. Real-Time TD-DFT Simulations in Dye Sensitized Solar Cells: The Electronic Absorption Spectrum of Alizarin Supported on TiO_2 Nanoclusters. *J. Chem. Theory Comput.* **2010**, *6*, 2856−2865.
(66) Qu, Z.-W.; Kroes, G.-J. Theoretical Study of The Electronic Structure and Stability of Titanium Dioxide Clusters $(TiO_2)_n$ with n = 1−9. *J. Phys. Chem. B* **2006**, *110*, 8998−9007.
(67) Tuikka, M.; Hirva, P.; Rissanen, K.; Korppi-Tommola, J.; Haukka, M. Halogen Bonding—A Key Step in Charge Recombination of The Dye-Sensitized Solar Cell. *Chem. Commun.* **2011**, *47*, 4499−4501.